British Journal of Pharmacology

DOI:10.1111/j.1476-5381.2012.01909.x
www.brjpharmacol.org

RESEARCH PAPER

# The gasotransmitter hydrogen sulphide decreases $Na^+$ transport across pulmonary epithelial cells

M Althaus[1], KD Urness[1], WG Clauss[1], DL Baines[2] and M Fronius[1]

[1]*Institute of Animal Physiology, Justus-Liebig University of Giessen, Giessen, Germany, and*
[2]*Division of Biomedical Sciences, St George's University of London, London, UK*

**Correspondence**
Dr Mike Althaus, Institute of Animal Physiology, Justus-Liebig University of Giessen, Heinrich-Buff-Ring 26, D-35392 Giessen, Germany. E-mail: mike.althaus@bio.uni-giessen.de

**Keywords**
sodium absorption; lung; ENaC; $Na^+/K^+$-ATPase; sodium channel; ion transport

**Received**
5 January 2012
**Revised**
2 February 2012
**Accepted**
3 February 2012

## BACKGROUND AND PURPOSE

The transepithelial absorption of $Na^+$ in the lungs is crucial for the maintenance of the volume and composition of epithelial lining fluid. The regulation of $Na^+$ transport is essential, because hypo- or hyperabsorption of $Na^+$ is associated with lung diseases such as pulmonary oedema or cystic fibrosis. This study investigated the effects of the gaseous signalling molecule hydrogen sulphide ($H_2S$) on $Na^+$ absorption across pulmonary epithelial cells.

## EXPERIMENTAL APPROACH

Ion transport processes were electrophysiologically assessed in Ussing chambers on H441 cells grown on permeable supports at air/liquid interface and on native tracheal preparations of pigs and mice. The effects of $H_2S$ were further investigated on $Na^+$ channels expressed in *Xenopus* oocytes and $Na^+/K^+$-ATPase activity *in vitro*. Membrane abundance of $Na^+/K^+$-ATPase was determined by surface biotinylation and Western blot. Cellular ATP concentrations were measured colorimetrically, and cytosolic $Ca^{2+}$ concentrations were measured with Fura-2.

## KEY RESULTS

$H_2S$ rapidly and reversibly inhibited $Na^+$ transport in all the models employed. $H_2S$ had no effect on $Na^+$ channels, whereas it decreased $Na^+/K^+$-ATPase currents. $H_2S$ did not affect the membrane abundance of $Na^+/K^+$-ATPase, its metabolic or calcium-dependent regulation, or its direct activity. However, $H_2S$ inhibited basolateral calcium-dependent $K^+$ channels, which consequently decreased $Na^+$ absorption by H441 monolayers.

## CONCLUSIONS AND IMPLICATIONS

$H_2S$ impairs pulmonary transepithelial $Na^+$ absorption, mainly by inhibiting basolateral $Ca^{2+}$-dependent $K^+$ channels. These data suggest that the $H_2S$ signalling system might represent a novel pharmacological target for modifying pulmonary transepithelial $Na^+$ transport.

## Abbreviations

ALI, acute lung injury; AMPK, adenosine monophosphate-activated protein kinase; ARDS, acute respiratory distress syndrome; $BK_{Ca}$, large conductance $K_{Ca}$ channel; CBS, cystathionine-β-synthase; CO, carbon monoxide; CPA, cyclopiazonic acid; CSE, cystathionine-γ-lyase; DMSO, dimethyl sulfoxide; DNP, 2,4-dinitrophenol; ENaC, epithelial $Na^+$ channel; FCS, fetal calf serum; Glib., glibenclamide; Go6983, 3-[1-[3-(dimethylamino)propyl]-5-methoxy-1H-indol-3-yl]-4-(1H-indol-3-yl)-1H-pyrrole-2,5-dione; $H_2S$, hydrogen sulfide; H-7, (+/–)-1-(5-isoquinolinesulfonyl)-2-methylpiperazine; $I_{ami}$, amiloride-sensitive current; $IK_{Ca}$, intermediate $K_{Ca}$ channel; $I_{lido}$, lidocaine-sensitive current; $I_{NaHS}$, NaHS-sensitive current; $I_{ouab}$, ouabaine-sensitive current; $I_{SC}$, short-circuit current; $K_{ATP}$, ATP-dependent $K^+$ channel; $K_{Ca}$, calcium-dependent $K^+$ channel; $K_V$, voltage-dependent $K^+$ channel; $R_T$, transepitehlial resistance; $SK_{Ca}$, short conductance $K_{Ca}$ channel; TBS, tris-buffered saline; TPeA, tetrapentylammonium; $V_T$, transepithelial potential; XE991, 10,10-bis(4-pyridinylmethyl)-9(10H)-anthracene

## Introduction

$Na^+$ absorption by pulmonary epithelia is crucial for the maintenance of lung fluid homeostasis. $Na^+$ ions apically enter the pulmonary epithelial cells through amiloride-sensitive $Na^+$ channels, such as the epithelial $Na^+$ channel (ENaC) (Matalon *et al.*, 2002), or amiloride-insensitive $Na^+$ channels, such as the cyclic nucleotide-gated channel A1 (CNGA1) (Wilkinson *et al.*, 2011). The $Na^+$ ions are extruded at the basolateral membrane of the epithelium by the activity of the $Na^+/K^+$-ATPase, consequently leading to the net movement of $Na^+$ ions from the apical to the basolateral side of the epithelium. This transepithelial $Na^+$ transport results in an osmotic gradient across the epithelium and is thus the main driving force for transepithelial fluid absorption.

Disregulated $Na^+$ transport across pulmonary epithelia is associated with lung diseases that are characterized by disturbed fluid homeostasis. Decreased $Na^+$ transport, especially across the alveolar epithelium, can, due to impaired alveolar fluid clearance, promote the development of pulmonary oedema (Althaus *et al.*, 2011). In the airways, ENaC hypoactivity, as in type 1 pseudohypoaldosteronism, will lead to increased volume of the airway lining fluid (Kerem *et al.*, 1999). By contrast, hyperactive $Na^+$ transport, especially in the airway epithelia, produces mucus thickening and cystic fibrosis-like lung disease (Mall *et al.*, 2004). Consequently, novel therapeutic strategies for the treatment of those diseases currently focus on a pharmacological intervention of $Na^+$ transport, and its regulation in the respiratory system (Althaus *et al.*, 2011; Becq *et al.*, 2011). Therefore, it is important to explore novel regulators of pulmonary transepithelial $Na^+$ transport, and thus identify novel putative pharmacological targets.

Recently, there is a growing body of evidence that small gas molecules, so called gasotransmitters, may regulate transepithelial ion transport processes. It was recently shown that the classical gasotransmitters NO and CO both decrease pulmonary transepithelial $Na^+$ transport: Whereas NO decreases the activity of amiloride-sensitive $Na^+$ channels as well as of the $Na^+/K^+$-ATPase (Guo *et al.*, 1998; Helms *et al.*, 2008; Althaus *et al.*, 2010), CO solely decreases the activity of amiloride-sensitive $Na^+$ channels in the lung (Althaus *et al.*, 2009). Besides NO and CO, hydrogen sulphide ($H_2S$), a gas with the characteristic odour of rotten eggs, has been suggested to be another gasotransmitter (Wang, 2002), that influences a variety of cellular and organ functions (for detailed review, see Olson, 2011). $H_2S$ is endogenously generated in humans from cysteine, mainly by the enzymes cystathionine-β-synthase (CBS) and cystathionine-γ-lyase (CSE) (Stipanuk and Beck, 1982; Wang, 2002). $H_2S$ production has also been demonstrated in lung tissue homogenates (Olson *et al.*, 2010).

In the respiratory system, $H_2S$ has profound vasoactive and anti-inflammatory effects (Olson, 2011). It mimics the vasoactive effects of hypoxia (Olson *et al.*, 2010), and administration of the $H_2S$-donating drug NaHS causes relaxation of mouse bronchial smooth muscle cells (Kubo *et al.*, 2007). $Na_2S$, another $H_2S$-donating molecule, reduces mortality and lung damage in a burn- and smoke-induced acute lung injury (ALI) model (Esechie *et al.*, 2009). NaHS also reduces inflammation in a rat model of ventilator-induced lung injury (VILI) (Aslami *et al.*, 2010). Inhaled $H_2S$ gas has beneficial effects in a rat model of VILI, which is due to inhibition of pro-inflammatory cytokine release and apoptosis (Faller *et al.*, 2010). Similar to the gasotransmitter CO (Ryter *et al.*, 2007), $H_2S$ is therefore suggested as a potential therapeutic option for the treatment of inflammatory lung diseases, including ALI (Esechie *et al.*, 2009; Otulakowski and Kavanagh, 2010).

Although there are currently no studies that have investigated the effect of $H_2S$ on pulmonary epithelia, evidence for regulation of transepithelial ion transport processes by $H_2S$ comes from studies on rat distal colonic preparations, where an increased $Cl^-$ secretion is observed after administration of NaHS (Hennig and Diener, 2009; Pouokam and Diener, 2011). However, whether or not $H_2S$ affects transepithelial $Na^+$ transport processes, is currently unknown.

The present study investigated the effect of $H_2S$ on $Na^+$ transport by a human airway line (H441), native tracheal preparations of pigs and mice and on $Na^+$ transporting molecules *in vitro* and in an heterologous expression system. These studies revealed that $H_2S$ decreases transepithelial $Na^+$ transport indirectly by inhibiting basolateral calcium-dependent $K^+$ channels. These data suggest that the $H_2S$ signalling system might represent a novel pharmacological target for the treatment of lung diseases that are associated with deregulated $Na^+$ and water homeostasis.

## Methods

### *Cell culture*

The H441 human bronchiolar epithelial cell line was purchased from the American Type Culture Collection (distributed by LGC Standards, Wesel, Germany) in the 65th passage. Cells were cultured in flasks with standard Roswell Park Memorial Institute culture medium containing 1640/L-glutamine medium (PAA, Cölbe, Germany), which was supplemented with 10% FCS (PAA), 1 mM $Na^+$ pyruvate, 1% insuline-transferrin-sodiumselenite medium supplement (Sigma, Taufkirchen, Germany) at 37°C in humidified atmosphere containing 5% $CO_2$. For Ussing chamber recordings, cells were removed from culture flasks using trypsin/EDTA (Sigma), resuspended in medium and seeded in confluent densities on permeable membrane supports (type 3801, Snapwell, Corning, Amsterdam, The Netherlands) under liquid/liquid conditions in standard medium supplemented with 1% antibiotic/antimycotic mix (Sigma). One day after seeding the medium on the apical side was aspired, and the basolateral medium was supplemented with 200 nM dexamethasone (Sigma). Medium was changed every 48 h. The cells were cultured for an additional 7 days under air/liquid conditions in the presence of dexamethasone. The monolayers were used for Ussing chamber studies from day 8 onwards.

### *Native tracheal tissue preparations*

Native tracheal epithelial preparations were freshly prepared from pigs and mice. Tracheae of pigs were obtained from a local butcher and kept at 4°C until the experiments were performed. The tracheae were incised longitudinally and the tissue containing the epithelium was dissected from the cartilage. The preparations were placed between two plastic rings

and mounted into Ussing chambers. Ussing chamber experiments were performed exactly as described later.

Adult mice (C57/Bl/6) were obtained from the local animal breeding facility (Justus-Liebig University of Giessen). Animals were killed by isoflurane overdose followed by aortic exsanguinations. The preparation of the tracheae and Ussing chamber recordings were performed exactly as described in Hollenhorst *et al*. (2012). The results of all studies involving animals are reported in accordance with the ARRIVE guidelines reporting experiments involving animals (McGrath *et al*., 2010). Experiments were performed according to the current law on the protection of animals in Germany and the National Institutes of Health guidelines for the care and use of laboratory animals.

## Ussing chamber studies

Confluent monolayers, grown on membrane supports, or tracheal preparations were mounted in perfusion Ussing chambers and bathed from both sides with physiological saline containing 130 mM NaCl, 2.7 mM KCl, 1.5 mM $KH_2PO_4$, 1 mM $CaCl_2$, 0.5 mM $MgCl_2$, 10 mM HEPES and 10 mM glucose (37°C, pH 7.35, NaOH). For the detection of electrical parameters, custom-made Ag/AgCl electrodes with KCl/agar bridges were used to connect the chamber bath with the voltage-clamp amplifier (custom made). Monolayers were maintained under open-circuit conditions and the spontaneous transepithelial potential ($V_T$) was monitored until a stable value was reached (~15 min). The $V_T$ was then clamped to 0 mV by the voltage-clamp amplifier, and short-circuit current ($I_{SC}$) was monitored (strip-chart recorder, Kipp&Zonen, Delft, The Netherlands) and recorded online using an analogue/digital interface (National Instruments, München, Germany). In order to estimate transepithelial resistance ($R_T$), voltage pulses of 2.5 mV were applied to the monolayers. The resulting current deflections were used to calculate $R_T$ using Ohm's law. All experiments were performed at 37°C.

*Measurement of basolateral $K^+$ channels*. In order to measure current fluxes through basolateral $K^+$ channels, H441 monolayers in Ussing chambers were apically permeabilized with nystatin (75 μM) in the presence of solutions, which generated a $K^+$ gradient from the apical to the basolateral compartment. The apical solution contained 30 mM KCl, 100 mM $K^+$ gluconate, 1.5 mM $KH_2PO_4$, 11 mM calcium gluconate, 0.5 mM $MgSO_4$, 10 mM HEPES and 10 mM glucose (pH 7.35/KOH). In order to block epithelial sodium channels, the solution also contained amiloride (10 μM). The basolateral solution consisted of 30 mM NaCl, 100 mM $Na^+$ gluconate, 1.5 mM $KH_2PO_4$, 11 mM calcium gluconate, 0.5 mM $MgSO_4$, 10 mM HEPES and 10 mM glucose (pH 7.35/NaOH). The solution also contained ouabain (1 mM) in order to block the $Na^+/K^+$-ATPase.

## Patch-clamp studies

For Patch-clamp studies, H441 cells were seeded in culture dishes (Thermo Scientific, Langenselbold, Germany) in standard culture medium. One day after seeding, 200 nM dexamethasone was added to the medium. After 48–72 h of dexamethasone exposure, whole-cell patch-clamp experiments were performed on single cells, which were located within small groups of cells. For experiments, culture dishes were washed with bath solution containing 140 mM NaCl, 4.5 mM KCl, 2.5 mM $CaCl_2$, 1 mM MgCl, 10 mM HEPES and 5 mM D-glucose (pH 7.4). Patch-pipettes were pulled from borosilicate capillaries and filled with a solution containing 10 mM NaCl, 18 mM KCl, 92 $K^+$ gluconate, 0.5 mM MgCl, 1 mM EDTA and 10 mM HEPES (pH 7.2). Whole-cell recordings were performed with a HEKA EPC 9 patch-clamp amplifier (HEKA Electronics, Lambrecht, Germany) at a holding potential of –48 mV. Together with the liquid junction potential of the bath and pipette solutions employed this resulted in a membrane potential of –60 mV during experiments. Electrical signals were acquired by an ITC-16 interface with the HEKA Pulse software (version 8.77). Chemicals were directly applied to cells by a pressure-driven perfusion system (custom made with a compressor, valves and microtubings). Experiments were performed at room temperature.

## Heterologous expression of ENaC and two-electrode voltage clamp (TEVC) recordings

The effect of $H_2S$ on ENaC was investigated by the TEVC technique in the *Xenopus* oocyte expression system. The α, β, γ and δ ENaC subunits were previously cloned from human lung mRNA (Fronius *et al*., 2010; Wesch *et al*., 2010). Defolliculated *Xenopus* oocytes were injected with cRNA encoding the human αβγ ENaC or δβγ ENaC subunits (for oocyte preparation and cRNA injection see Fronius *et al*., 2010). The RNA concentration was 10 $ng \cdot \mu L^{-1}$ per subunit and a volume of 23 nL was injected per oocyte. Experiments were performed 24–48 h after injection. For this purpose, oocytes were placed in a lucite chamber and perfused by a gravity driven system with oocyte Ringer's solution, containing 90 mM NaCl, 1 mM KCl, 2 mM $CaCl_2$ and 10 mM HEPES (pH 7.4). Glass capillaries with an outer diameter of 1.2 mm were pulled to microelectrodes and filled with 1 M KCl. The membrane voltage was clamped to –60 mV using a TEVC amplifier (Warner Instruments, Hamden, CT, USA) and transmembrane currents ($I_M$) were continuously recorded with a strip chart recorder (Kipp&Zonen).

## $H_2S$ administration and chemicals used

Due to the high toxicity of $H_2S$ gas, the $H_2S$-donating drug NaHS (Sigma) was employed. In aqueous solution, NaHS dissociates into $Na^+$, $H_2S/HS^-$ and $OH^-$. Due to the formation of $OH^-$, buffers were adjusted to keep the pH stable over the time course of experiments. Stock solutions of NaHS were freshly prepared in water before each experiment. The final concentration of NaHS in Ussing chamber recordings was 300 μM, of which approximately one-third (100 μM) represents free $H_2S$ (Reiffenstein *et al*., 1992). For experiments that were performed at room temperature (patch clamp, voltage clamp and calcium imaging), a higher concentration of NaHS was employed (1 mM).

Unless indicated otherwise, all chemicals were obtained from Sigma. All inhibitors employed, their targets and concentrations are listed in Table 1. The nomenclature of drugs and targets conforms to BJP's Guide to Receptors and Channels (Alexander *et al*., 2011). Where necessary, drugs were dissolved in dimethyl sulfoxide (DMSO, Sigma) and control

**Table 1**
Purpose and concentrations of the inhibitors employed

| Substance | Purpose | C (M) | Company | References |
|---|---|---|---|---|
| Amiloride | ENaC inhibitor | $10^{-5}$ | Sigma | Canessa *et al.*, 1994 |
| Ouabain | $Na^+/K^+$-ATPase inhibitor | $10^{-3}$ | Sigma | Ramminger *et al.*, 2004; Woollhead *et al.*, 2007 |
| Lidocaine | Non-specific $K^+$ channel inhibitor | $3 \times 10^{-3}$ | Sigma | Inglis *et al.*, 2007 |
| Glibenclamide | $K_{ATP}$ channel inhibitor | $10^{-4}$ | Sigma | Barrett-Jolley and Davies, 1997; Hennig and Diener, 2009 |
| TPeA | $K_{Ca}$ channel inhibitor | $3 \times 10^{-4}$ | Sigma | Hennig and Diener, 2009; Maguire *et al.*, 1999 |
| XE991 | $K_V$ channel inhibitor | $10^{-4}$ | Biozol | Greenwood *et al.*, 2009; Wang *et al.*, 1998; 2000 |
| Dynasore | Dynamin-inhibitor | $7 \times 10^{-5}$ | Biozol | Macia *et al.*, 2006 |
| H-7 | Non-selective PKC inhibitor | $2 \times 10^{-5}$ | Biozol | Hidaka *et al.*, 1984 |
| Staurosporine | Non-selective PKC inhibitor | $2 \times 10^{-7}$ | Biozol | Rüegg and Burgess, 1989; Tamaoki *et al.*, 1986 |
| Go6983 | Broad spectrum PKC inhibitor | $5 \times 10^{-6}$ | Biozol | Gschwendt *et al.*, 1996 |
| PKC peptide inhibitor | PKC inhibitor | $6 \times 10^{-5}$ | Sigma | Eichholtz *et al.*, 1993 |

C, concentration; TPeA, tetrapentylammonium.

experiments were performed with analogous concentrations of DMSO. For permeabilization experiments, nystatin (Sigma) was used. This drug generates ion selective pores, which are permeable for monovalent ions such as $Na^+$, $K^+$ and $Cl^-$ (Russell *et al.*, 1977).

## *Surface biotinylation and Western blotting for the detection of membrane proteins*

Plasma membrane proteins were isolated and purified by the method described previously (Woollhead *et al.*, 2007; Tan *et al.*, 2011). Briefly, monolayers were transferred to ice, and both filter compartments rinsed with ice-cold PSS (pH 7.4). Biotinylation solution [1.5 mL of 0.5 mg·mL$^{-1}$ sulfo-N-hydroxysuccinimide-biotin (sulfo-NHS-biotin) in borate buffer pH 8.2] was added to the basolateral compartment and the monolayers incubated with gentle rocking for 30 min. Apical biotinylation was prevented by adding 500 µL PSS + 10% FBS to the apical chamber. The biotinylation solution was removed and PSS + 10% FBS was added to quench all unreacted sulfo-NHS-biotin groups, followed by three washes with PSS. Cells were then lysed, proteins solubilized, and the protein concentration was then determined by Bradford assay. Similar amounts of total protein were incubated overnight with streptavidin agarose beads at 4°C. The following day, biotinylated proteins bound to beads were separated from non-biotinylated proteins by centrifugation. Bound biotinylated proteins were eluted into 30 µL sample loading buffer by heating at 95°C for 5 min. Bound and unbound (30µg) proteins were separated by NuPAGE (Invitrogen, Paisley, UK) on 4–12% Bis-Tris gels, and transferred to low fluorescence PVDF membrane. Membranes were blocked for 1 h at room temperature in Odyssey blocking buffer (LI-COR, Lincoln, NE, USA), then incubated with primary antibodies overnight at 4°C. Membranes were washed in Tris buffered saline + 0.01% TWEEN, and incubated with a fluorescent secondary antibody diluted in Odyssey buffer for 1 h at room temperature. Proteins were visualized and band density analysed using the Odyssey system (LI-COR). Anti α1-$Na^+/K^+$ATPase monoclonal antibody was developed by D Fambrough and was obtained from the Developmental Studies Hybridoma Bank developed under the auspices of the National Institute of Child Health and Human Development maintained by the University of Iowa, USA. Anti beta-actin was obtained from Ab-cam (Cambridge, UK). Fluorescent secondary antisera were obtained from Odyssey (LI-COR).

## *Calcium imaging experiments*

Changes in cytosolic $Ca^{2+}$ concentrations were measured using Fura-2. For the experiments, H441 cells were seeded on glass cover slips and cultured in the presence of dexamethasone for 48–72 h. Cells were washed with PSS, and incubated for at least 45 min at 37°C with 2.5 µM Fura-2 AM (Invitrogen, Darmstadt, Germany) and 0.05% pluronic (20% solution in DMSO, Invitrogen). After incubation, cells were washed twice and perfused with PSS (5 mL·min$^{-1}$). NaHS (1 mM) and cyclopiazonic acid (CPA; 10 µM; Alexis, Grünberg, Germany or Biozol, Eching, Germany) were then applied via the perfusion system. Changes in cytosolic $Ca^{2+}$ concentrations were measured at room temperature as changes in the Fura-2 ratio (emission at an extinction of 340 nm divided by emission at an extinction of 380 nm) exactly as previously described (Pouokam and Diener, 2011).

## *Colometric determination of catalytic $Na^+/K^+$-ATPase activity*

The catalytic activity of the $Na^+/K^+$-ATPase was determined by a colometric assay (EC 3.6.1.3, Sigma). This *in vitro* assay is based on the measurement of the amount of inorganic phosphorous ($P_i$) that is liberated upon ATP hydrolysis by a purified $Na^+/K^+$-ATPase (Sigma). The reaction, with and without 1 mM NaHS, was performed exactly according to manufacturer's instructions. The supernatant of the enzyme reaction was used to determine the amount of inorganic phosphorus according to the method described by Taussky and Shorr (1953), by quantification at 660 nm with a spectrophotom-

eter (Kruess Optronic, Hamburg, Germany). The activity of the $Na^+/K^+$-ATPase was calculated by the subtraction of background activity, which was determined with the $Na^+/K^+$-ATPase inhibitor ouabain (1 mM). The total amount of $P_i$ was determined with a standard curve made from phosphorus standard solution (Sigma).

### Colorimetric determination of cellular ATP levels

For the determination of cellular ATP levels a colorimetric ATP assay kit (Abnova, Heidelberg, Germany) was used. H441 cells were cultured on permeable supports, as described for Ussing chamber experiments. Cells were apically exposed to 300 µL PSS, with or without NaHS (300 µM or 1 mM) for 15 min at 37°C and 5% $CO_2$ in humidified atmosphere. 2,4-Dinitrophenol (DNP; 500 µM; 30 min exposure) was used as a positive control. Because DNP was dissolved in DMSO, all solutions contained 0.1% DMSO. After incubation of the monolayer with the drugs described, cells were cooled to 4°C and all media were aspired. Afterwards, cells were frozen at –80°C. Cells were then thawed and lysed in 100 µL of ATP assay buffer as supplied by the manufacturer. Further sample preparation and colorimetric determination of ATP was performed exactly according to manufacturer's instructions by measuring the absorbance at 570 nm with a spectrophotometer (Kruess Optronic). ATP concentrations were estimated with an ATP standard curve.

### Statistics

Values are presented as mean ± SEM. For statistical analysis, mean values of unpaired experiments (e.g. parallel conducted controls and drug exposed monolayers from identical passages) were compared by Student's unpaired *t*-test. For the comparison of dependent means (e.g. before and after exposure to reagents), Student's paired *t*-test was used. For the statistical comparison of more than two groups, one-way ANOVA followed by Bonferroni's multiple comparison test was used. Statistical tests were performed with Microsoft Excel 2003 or GraphPad Prism versions 4 and 5. The number of experiments is indicated by *n*, which represents single H441 monolayers on permeable supports for Ussing chamber experiments; single cells from separate culture dishes for patch-clamp recordings; single oocytes injected with ENaC-encoding RNA; and single animals from which tracheae were obtained. In experiments with pig tracheal preparations, in total seven tissue preparations were made from three pigs and Ussing chamber studies were performed independently. All control experiments were performed from the same cell or oocyte preparations, for example, cells were derived for Ussing chamber cultures from the same culture flask, or oocytes were harvested from the same donor frog. *P*-values ≤ 0.05 were regarded to be significant, and marked in the figures by an asterisk (*).

## Results

### Effects of $H_2S$ on $Na^+$ absorption by H441 cells and native tracheal preparations

The effect of $H_2S$ on $Na^+$ absorption by pulmonary epithelial cells was investigated with the H441 human airway epithelial cell line. These cells have been demonstrated to represent a suitable model for electrophysiological ion transport studies, and exhibit a robust $Na^+$-absorbing phenotype when cultured at air/liquid interface in the presence of glucocorticoids (Lazrak and Matalon, 2003; Clunes *et al.*, 2004; Ramminger *et al.*, 2004; Woollhead *et al.*, 2005; Albert *et al.*, 2008; Brown *et al.*, 2008; Mace *et al.*, 2008; Althaus *et al.*, 2009; 2010; Nie *et al.*, 2009; Tan *et al.*, 2011). The administration of the $H_2S$-donating molecule, NaHS (300 µM, apical application), to H441 monolayers in Ussing chambers rapidly decreased transepithelial short-circuit currents from 12.8 ± 3 µA·cm$^{-2}$ to 6.0 ± 1.9 µA·cm$^{-2}$ ($P < 0.05$; $n = 5$) within 5 min (Figure 1A). Comparing the current-fractions sensitive to the ENaC blocker amiloride, before and after NaHS application, revealed that NaHS significantly decreased amiloride-sensitive currents ($I_{ami}$) by approximately 60% from 10.2 ± 1.8 µA·cm$^{-2}$ to 3.8 ± 0.9 µA·cm$^{-2}$ ($n = 5$; $P < 0.05$) (Figure 1A, B). To prove that the observed decreases in ion currents were not the result of damage to the monolayers, the effect of NaHS on transepithelial resistance, which would decrease upon epithelial damage, was measured (Figure 1C). Transepithelial resistance was 200.2 ± 25.4 Ω·cm$^{-2}$ before and 243.8 ± 25 Ω·cm$^{-2}$ after NaHS administration ($n = 5$; $P < 0.01$). In the presence of amiloride (10 µM), the effect of NaHS was lost (Figure 1D). $I_{SC}$ values, in the presence of amiloride, were 5 ± 2.7 µA·cm$^{-2}$ before, and 5.75 ± 2.8 µA·cm$^{-2}$ after NaHS ($n = 4$; $P = 0.06$). The effect of NaHS on $I_{ami}$ was concentration-dependent, with an $IC_{50}$ of 146 µM ($n = 3$; Figure 1E). Interestingly, the effect of NaHS on $I_{ami}$ was rapidly reversed after wash-out of the drug (Figure 1F, G). Values of $I_{ami}$ before NaHS application (8.33 ± 1 µA·cm$^{-2}$) and after washout (6.4 ± 1.5 µA·cm$^{-2}$) were not significantly different ($n = 7$; $P = 0.1$).

In addition, the effect of NaHS on $I_{ami}$ was also investigated on native tracheal preparations of pigs and mice in Ussing chambers (Figure 2). The administration of NaHS reversibly reduced $I_{ami}$ of pig tracheae (Figure 2A, B) by 52 ± 10% ($n = 3$, $P < 0.01$). Similar results were obtained from recordings on mice tracheae (Figure 2C, D), where NaHS reversibly decreased $I_{ami}$ by 66 ± 3% ($n = 3$, $P < 0.01$).

### Effect of $H_2S$ on cellular ATP levels

An important cellular target for $H_2S$ is the mitochondrial respiratory chain. It has previously been demonstrated that $H_2S$ can reversibly inhibit cytochrome c oxidase (Collman *et al.*, 2009), which eventually leads to metabolic depletion of cells. Because the activity of $Na^+/K^+$-ATPase is tightly linked to cellular ATP levels, it may be speculated that $H_2S$ inhibits $I_{ami}$ indirectly by decreasing the concentration of cellular ATP. ATP concentrations of H441 monolayers, which were incubated with or without NaHS for 15 min, were therefore measured with a colorimetric approach. Control monolayers contained 18.35 ± 0.68 µM ATP ($n = 5$), which was not significantly different from monolayers treated with 300 µM NaHS (16.51 ± 1.27 µM ATP; $n = 6$, one-way ANOVA) or 1 mM NaHS (18.07 ± 0.58 µM ATP; $n = 6$, one-way ANOVA). The mitochondrial uncoupler 2,4-DNP significantly decreased ATP levels to 13.42 ± 0.78 µM ($n = 6$, $P < 0.05$, one-way ANOVA), which indicates that changes in ATP concentrations could be detected with the setup employed.

In general, transepithelial $Na^+$ transport is the result of the interplay of mainly two $Na^+$-transporting molecules in epi-

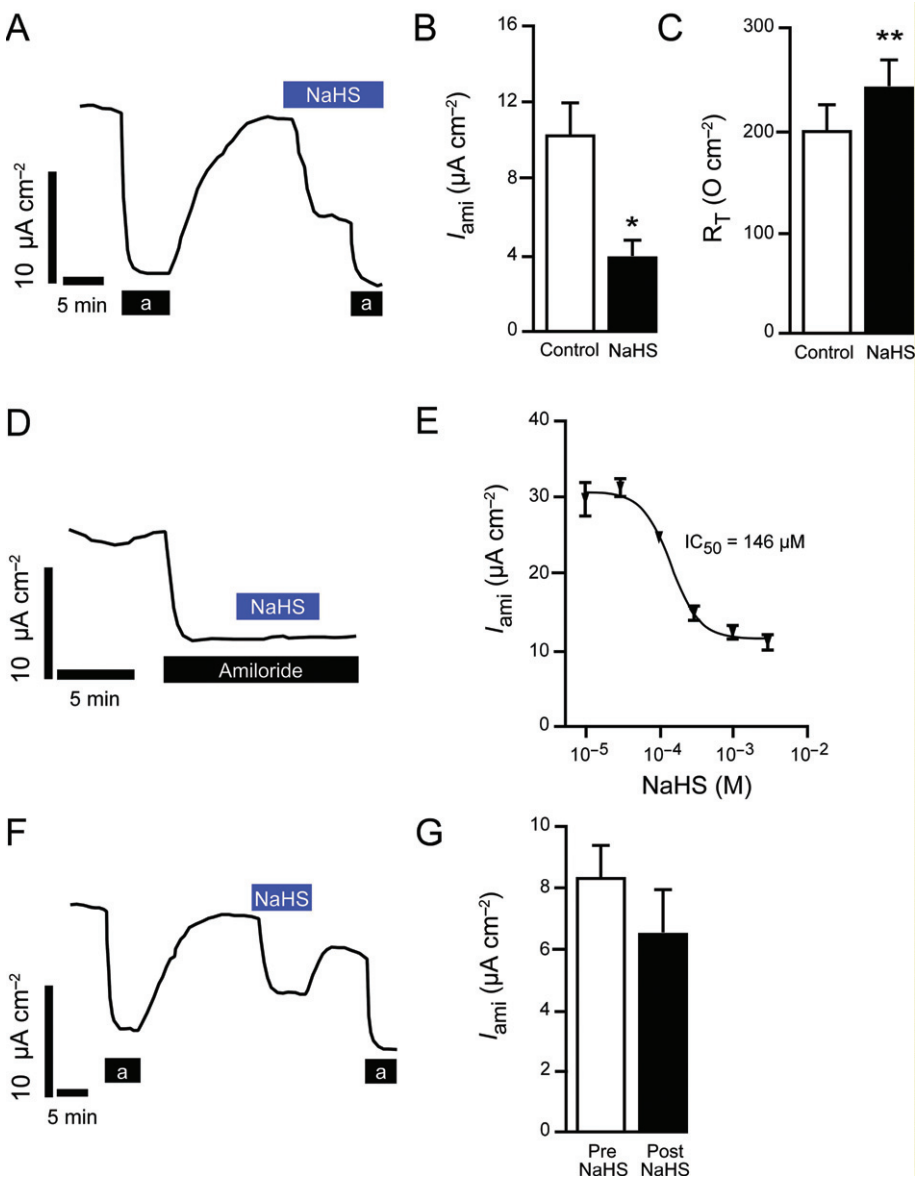


## Figure 1

Effects of NaHS on $Na^+$ absorption by H441 monolayers. (A) Representative current trace. First, amiloride (10 µM, indicated with 'a') was applied to the apical bath to estimate baseline amiloride-sensitive $Na^+$ currents. After wash-out of amiloride, NaHS (300 µM) was applied to the apical bath (blue bar), which resulted in a rapid current decrease. After 5 min, amiloride (10 µM) was applied. (B) Statistical analysis of experiments shown in (A). Depicted are amiloride-sensitive currents ($I_{ami}$) that were obtained from differences in current values before and after application of amiloride. (C) Transepithelial resistance ($R_T$) was not decreased by NaHS. (D) In the presence of amiloride, there was no effect of NaHS on short-circuit currents. (E) NaHS concentration-dependently decreased $I_{ami}$. Data were obtained from H441 monolayers exposed to different concentrations of NaHS ($n = 3$ for each concentration). The $IC_{50}$ value was obtained from a sigmoidal concentration-response fit according to the Hill equation. (F) Reversibility of the NaHS effect. Experiments started analogous to those shown in (A). After removal of NaHS, currents nearly increased back to baseline levels. Amiloride was applied again and the $I_{ami}$ values before and after NaHS were statistically compared (G). *$P < 0.05$; **$P < 0.01$.

thelial cells: $Na^+$ channels located at the apical membrane of the epithelial cells and the $Na^+/K^+$-ATPase located at the basolateral membrane. Inhibition of either transport system will decrease overall transepithelial $Na^+$ transport. Therefore, experiments were performed to elucidate whether the observed inhibition of $I_{ami}$ by NaHS was due to inhibition of amiloride-sensitive $Na^+$ channels, such as ENaC, or inhibition of the $Na^+/K^+$-ATPase.

### *Effects of $H_2S$ on amiloride-sensitive $Na^+$ channels*

To investigate if NaHS inhibits amiloride-sensitive $Na^+$ channels, whole-cell patch-clamp experiments were performed on single H441 cells (Figure 3A, B). The application of amiloride (100 µM) decreased approximately 80% of the inward current at –60 mV holding potential. The amiloride-sensitive fraction

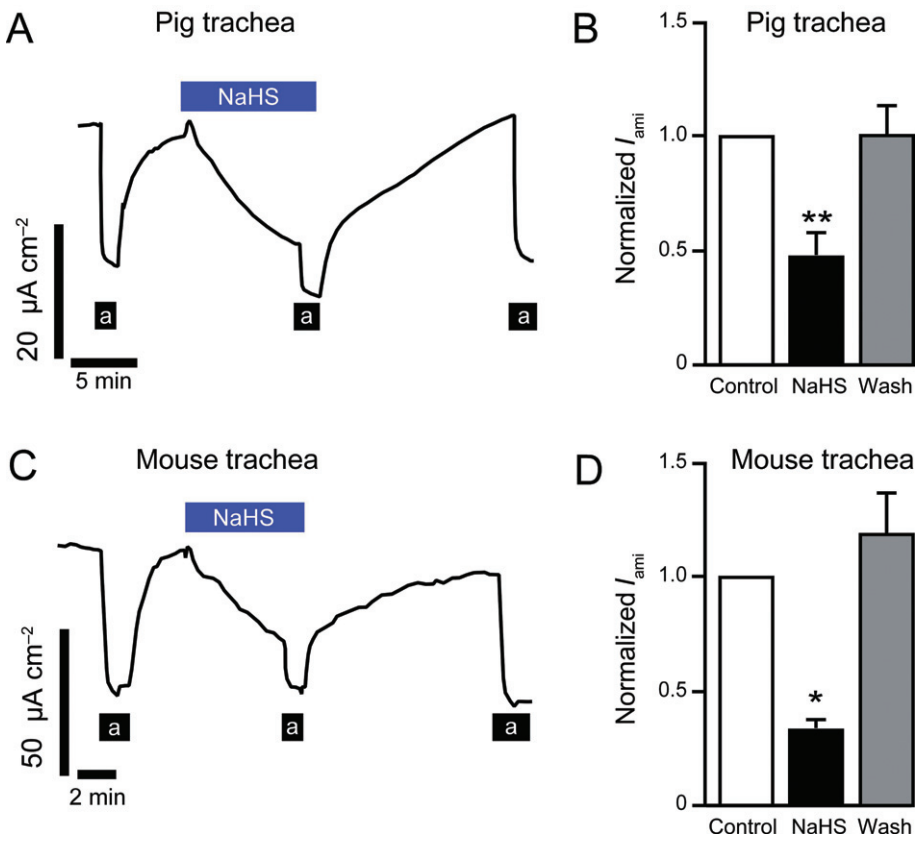


## Figure 2

Effects of NaHS on $Na^+$ absorption by native tracheal preparations. (A) Original current trace of an Ussing chamber recording of native tracheal epithelium from pig. First, baseline amiloride-sensitive currents were estimated with amiloride (10 µM, a). After wash-out, NaHS (300 µM, apical side) was applied for 8 min, and then amiloride was applied. After 15 min of wash-out, amiloride was applied again. (B) Statistical analysis from experiments shown in (A). Depicted are normalized values of amiloride-sensitive currents ($I_{ami}$) that were obtained as ratios from values of $I_{ami}$ with respect to baseline $I_{ami}$. NaHS significantly decreased $I_{ami}$ ($n = 3$, $^{**}P < 0.01$). Furthermore, after wash-out of NaHS, values of $I_{ami}$ increased again and were not significantly different from baseline levels ($n = 3$, $P = 0.95$). (C, D) Similar experiments as shown in (A and B) on native tracheal preparations of mice ($n = 3$). NaHS also significantly reduced $I_{ami}$ within 5 min ($n = 3$, $^{*}P < 0.01$). After wash-out of NaHS, $I_{ami}$ was not significantly different from baseline levels ($n = 3$, $P = 0.4$).

($I_{ami}$), however, was not affected by the administration of NaHS (1 mM). Normalized values of $I_{ami}$ were 0.81 ± 0.12 under control conditions, and 0.83 ± 0.17 after NaHS exposure ($n = 6$; $P = 0.92$). These data indicate that NaHS does not inhibit amiloride-sensitive $Na^+$ channels in H441 cells. To confirm this observation, TEVC recordings were performed on *Xenopus* oocytes, which expressed combinations of amiloride-sensitive ENaC subunits (Figure 3C, D). The classical ENaC consists of three subunits, α, β and γ, which probably assemble as a trimer in the plasma membrane (Jasti *et al.*, 2007). However, an additional subunit, δ, is expressed – at least at the mRNA level – in H441 cells (Wesch *et al.*, 2010), which can also form robust amiloride-sensitive $Na^+$ currents when co-expressed with β and γ (Wesch *et al.*, 2010). The administration of NaHS (1 mM), however, did not affect the $I_{ami}$ of oocytes expressing either the amiloride-sensitive αβγ or δβγ subunits of ENaC. Normalized values of $I_{ami}$ for the αβγENaC expressing oocytes were 0.96 ± 0.05 under control conditions, and 0.88 ± 0.07 after NaHS exposure ($n = 8/9$; $P = 0.37$). Values for δβγENaC expressing oocytes were 1.0 ± 0.02 (control) and 1.07 ± 0.05 (NaHS; $n = 7$; $P = 0.25$).

### *Effects of $H_2S$ on basolateral $Na^+/K^+$-ATPase currents of H441 monolayers*

As NaHS had no effect on amiloride-sensitive $Na^+$ channels, it was hypothesized that NaHS, instead, impairs the activity of the basolaterally located $Na^+/K^+$-ATPase. Given that $H_2S$ is membrane permeable (Mathai *et al.*, 2009), it is reasonable to assume apically applied $H_2S$ has an effect on a basolateral enzyme. To test this hypothesis, the effect of NaHS on functionally isolated basolateral membranes of H441 monolayers was investigated in Ussing chambers (Figure 4). Firstly, amiloride was applied to the apical bath to block apical $Na^+$ channels. Then, nystatin (75 µM) was added to the apical bath to permeabilize the apical membrane. This resulted in an increase in $I_{SC}$, which is mainly generated by the $Na^+/K^+$-ATPase (Woollhead *et al.*, 2007; Althaus *et al.*, 2009; 2010). When the current was stable, ouabain (1 mM), an inhibitor of the $Na^+/K^+$-ATPase, was applied to the basolateral bath, which

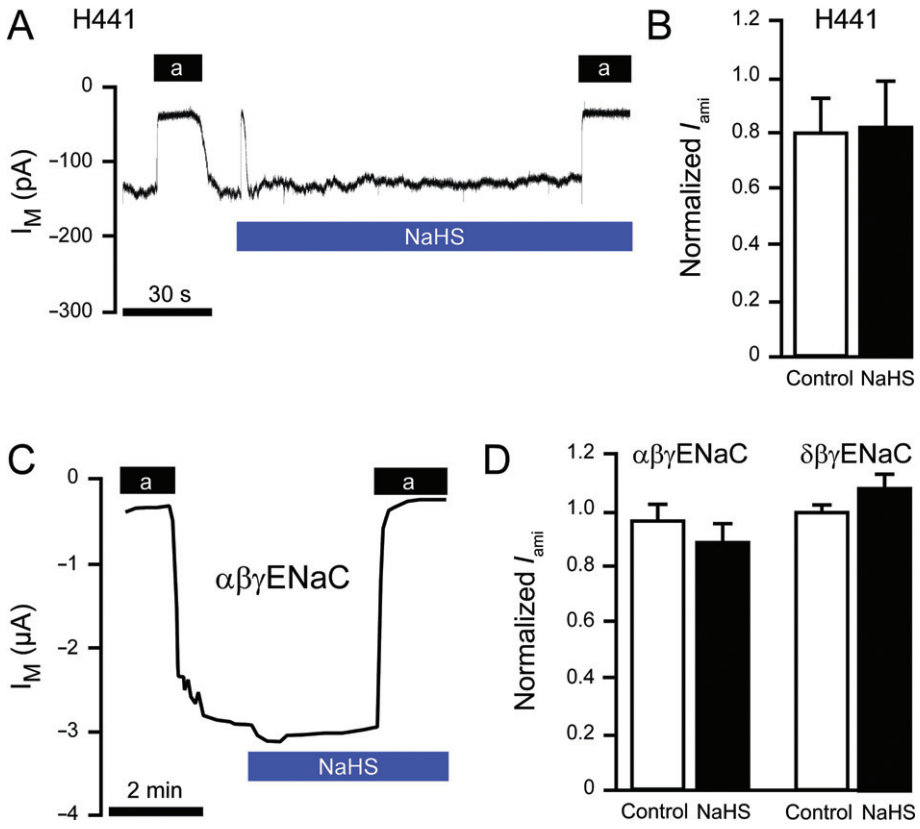


## Figure 3

Effects of NaHS on amiloride-sensitive sodium channels. (A) Original transmembrane current ($I_M$) trace from a whole-cell patch clamp recording of a single H441 cell. The holding potential was –60 mV. Amiloride-sensitive $Na^+$ currents were estimated by the application of amiloride (100 μM, indicated with 'a'). After wash-out of amiloride, NaHS (1 mM, blue bar) was applied. After 2 min of NaHS exposure, amiloride was applied. The transient current decrease upon NaHS application represents an artefact by the perfusion system, which was also present in control recordings without NaHS (data not shown). (B) Statistical evaluation of experiments shown in (A). Depicted are normalized amiloride-sensitive currents (normalized $I_{ami}$), which were obtained by the ratio of amiloride-sensitive currents after exposure, to either vehicle (control, recording not shown) or NaHS, to the baseline amiloride-sensitive current (estimated at the beginning of each experiment). (C) Representative current trace of a TEVC recording that investigated the effect of NaHS on heterologously expressed αβγENaCs in *Xenopus* oocytes. Experiments started with the perfusion of amiloride (10 μM). After wash-out of amiloride, $I_M$ increased, which represents ENaC activity. The application of NaHS (1 mM) had no effect on $I_M$. After exposure to NaHS, amiloride was applied again. (D) Statistical evaluation of experiments shown in (C). Shown are means of normalized $I_{ami}$. Normalization was as described in (B). There was no effect of NaHS on normalized $I_{ami}$ of oocytes expressing either αβγENaC or δβγENaC.

resulted in a large decrease in the $I_{SC}$ (Figure 4A). The difference in $I_{SC}$ values before and after addition of ouabain represents the activity of the $Na^+/K^+$-ATPase ($I_{ouab}$). $I_{ouab}$ values were 13.8 ± 0.49 μA·cm$^{-2}$ in control experiments, and 5.8 ± 0.58 μA·cm$^{-2}$ in experiments where NaHS was applied before ouabain ($n$ = 5, $P$ < 0.01) (Figure 4B, C). This indicates that NaHS led to a decrease in $Na^+/K^+$-ATPase activity by approx. 60%.

### *Measurement of membrane abundance of the $Na^+/K^+$-ATPase*

Changing the abundance of transporting molecules in the plasma membrane of epithelial cells is a general mechanism that regulates transepithelial ion transport processes. The observed inhibition of $Na^+/K^+$-ATPase currents in H441 monolayers might thus be due to NaHS-induced internalization of $Na^+/K^+$-ATPase molecules from the basolateral plasma membrane.

The abundance of $Na^+/K^+$-ATPase proteins in the basolateral membrane was investigated using a surface protein biotinylation approach followed by Western blotting (Figure 5A, B). There were no significant changes in membrane abundance of the $Na^+/K^+$-ATPase, even after a 60-min incubation with NaHS. This finding was confirmed by Ussing chamber studies with an endocytosis inhibitor (dynasore; Figure 5C). Pretreatment of monolayers with dynasore (70 μM, 1 h incubation) did not significantly affect $I_{NaHS}$ (6.0 ± 1.29 μA·cm$^{-2}$) compared with control experiments (DMSO-treated monolayers; (8.0 ± 2.12 μA·cm$^{-2}$; $n$ = 4; $P$ = 0.46).

### *Effects of $H_2S$ on cytosolic $Ca^{2+}$ concentrations and $Na^+/K^+$-ATPase activity*

As there was no detectable change in the abundance of the $Na^+/K^+$-ATPase in the membrane, $H_2S$ may instead affect $Na^+/K^+$-ATPase activity. In previous studies it has been demon-

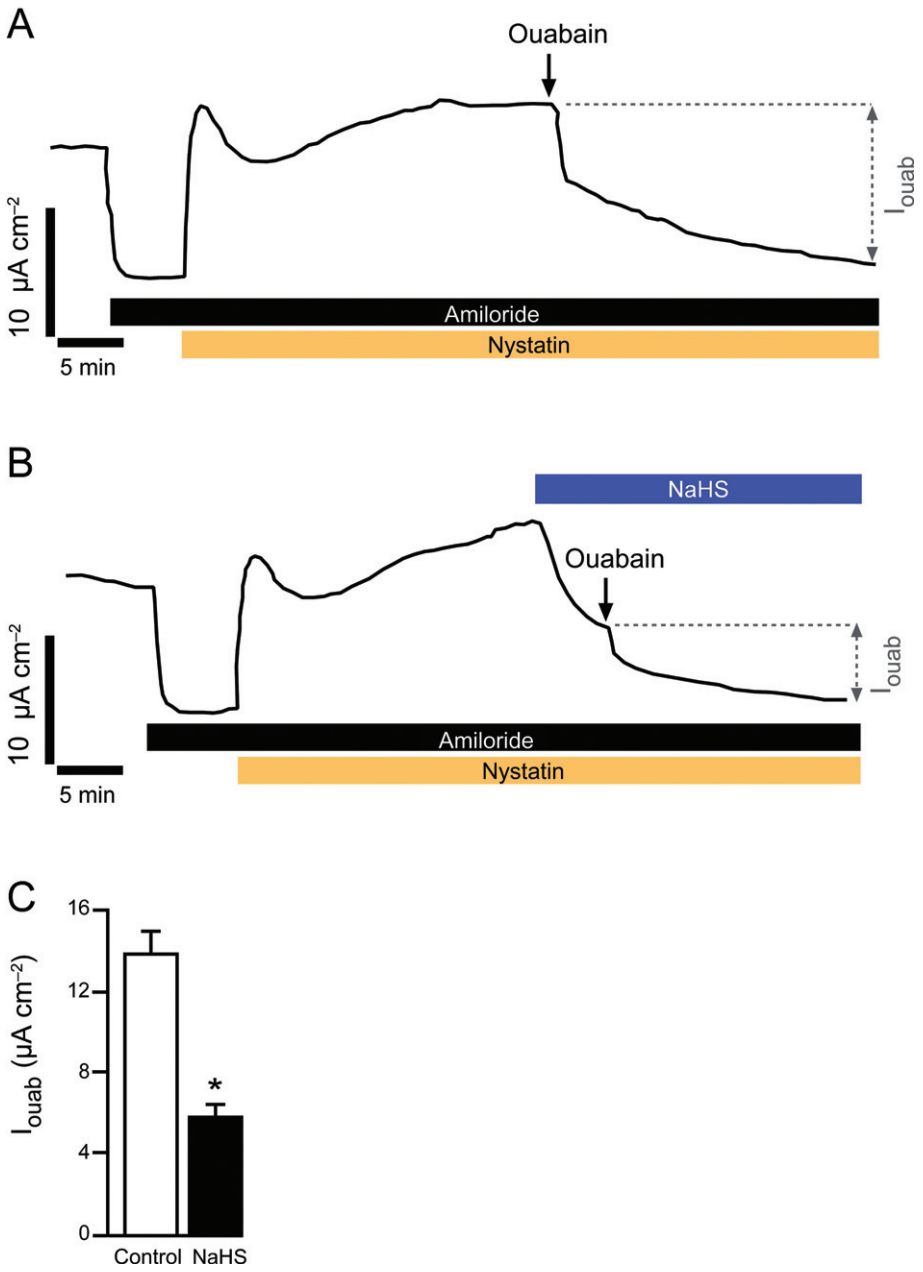


## Figure 4

Effects of NaHS on basolateral $Na^+/K^+$-ATPase activity in H441 monolayers. (A) Representative current trace of apically permeabilized H441 monolayers in Ussing chambers. Firstly, amiloride (10 µM) was applied to block apical ENaCs. Nystatin (75 µM, yellow bar) was subsequently applied to the apical bath. The resulting increase in short-circuit current ($I_{SC}$) represents the activity of the basolateral $Na^+/K^+$-ATPase. $Na^+/K^+$-ATPase activity was finally measured as $I_{SC}$ values sensitive to the basolateral application of ouabain (1 mM), and denoted $I_{ouab}$. (B) Similar experiment to that shown in (A). After permeabilization with nystatin, NaHS (300 µM) was apically applied, which resulted in a current decrease. Note the current fraction, which is sensitive to ouabain, is decreased compared with the experiment as shown in (A). (C) Statistical analysis of experiments as shown in (A and B). $I_{ouab}$ values without and with NaHS were compared. *$P < 0.01$.

strated that $H_2S$ elicits $Ca^{2+}$ signals (Lee *et al.*, 2006; Pouokam and Diener, 2011) that may activate downstream PKC and thereby decrease the activity of the $Na^+/K^+$-ATPase (Bertorello *et al.*, 1991).

Putative changes in cytosolic $Ca^{2+}$ concentrations of H441 cells were measured using Fura-2 (Figure 6). The application of NaHS (1 mM) led to a slight and reversible increase in Fura-2 ratios from 0.472 ± 0.007 to 0.557 ± 0.011 ($n = 40$; $P < 0.01$; Figure 6). CPA (10 µM), which was used as a positive control and inhibits sarcoplasmic reticulum $Ca^{2+}$-ATPase, led to a strong increase in Fura-2 ratios from 0.47 ± 0.007 to 0.868 ± 0.041 ($n = 40$; $P < 0.01$; Figure 6).

As NaHS increased cytosolic $Ca^{2+}$ concentrations, different inhibitors of $Ca^{2+}$-dependent PKC were employed (Figure 7).

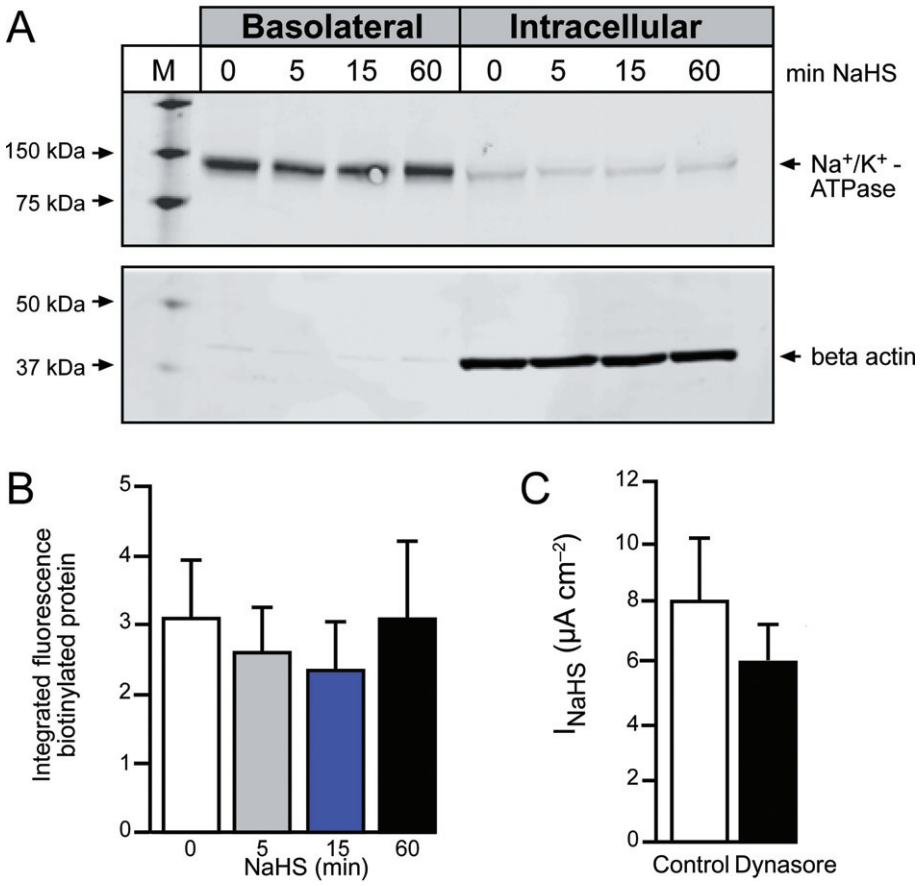


## Figure 5

Effects of NaHS on the abundance of $Na^+/K^+$-ATPase in the membrane. (A) Western blot showing the abundance of $Na^+/K^+$-ATPase, in the basolateral membrane (basolateral) or in the non-bound predominantly intracellular protein fraction (intracellular), after different exposure times to NaHS (1 mM). As a control, the same blot was analysed for β actin, which should only be present in the intracellular fraction and not in the basolateral biotinylated fraction. (B) Graph of biotinylated $Na^+/K^+$-ATPase protein abundance by using integrative fluorescence analysis of Oddysey images from $n = 5$ independent samples. There was no significant difference between groups ($n = 5$; $P = 0.8991$, one-way ANOVA). (C) Data from Ussing chamber experiments that were performed with the endocytosis inhibitor dynasore. Monolayers were incubated with dynasore (70 µM, 1 h incubation) or DMSO (control) and the NaHS-induced current decrease ($I_{NaHS}$) was compared.

However, there were no significant changes in NaHS-induced currents when H441 monolayers were pretreated with Go6983 (5 µM; Figure 7A–C), staurosporine (200 nM; Figure 7C), a myristoylated PKC peptide inhibitor (60 µM; Figure 7D), or H-7 (20 µM; Figure 7E). Further, the application of CPA (10 µM, apical application), which strongly increased cytosolic calcium concentrations in H441 cells (Figure 6), did not significantly change amiloride-sensitive $Na^+$ currents (Figure 7F, G). Values of $I_{ami}$ were 22.2 ± 1.53 µA·cm$^{-2}$ before, and 22.7 ± 1.67 µA·cm$^{-2}$ after administration of CPA ($n = 5$; $P = 0.41$; Figure 8F, G).

In addition, the activity of purified $Na^+/K^+$-ATPase (from porcine brain) was determined by measuring ouabain-sensitive production of inorganic phosphorus due to ATP hydrolysis. Under control conditions, purified $Na^+/K^+$-ATPase liberated 60.01 ± 9.7 µM of phosphorus within 15 min at 37°C. This was not significantly different from the amount of phosphorus that was released in the presence of 1 mM NaHS (59.67 ± 1.98 µM; $n = 5$, $P = 0.97$).

### *Modulation of basolateral $K^+$ channels and its effects on transepithelial $Na^+$ transport*

Important regulators of transepithelial $Na^+$ transport, including the $Na^+/K^+$-ATPase, are $K^+$ channels, which are located in the basolateral membrane of epithelial cells. Basolateral $K^+$ channels critically affect the membrane potential of the apical membrane and are important for the recycling of $K^+$ ions, which are pumped into the cells by the $Na^+/K^+$-ATPase (Greenwood *et al.*, 2009). Thus, an inhibition of $K^+$ channel activity will decrease transepithelial $Na^+$ transport processes due to impairment of electrochemical gradients in the epithelial cells.

The activity of the $Na^+/K^+$-ATPase was measured by apical permeabilization exactly as described earlier (Figure 8). Under these conditions, basolateral application of the non-selective $K^+$ channel inhibitor lidocaine (3 mM) decreased the ouabain-sensitive fraction of the $I_{SC}$, $I_{ouab,}$ from 11.5 ± 1.7 µA·cm$^{-2}$ to 6.8 ± 1.2 µA·cm$^{-2}$ ($n = 5$, $P = 0.05$; Figure 8A, B). Additionally,

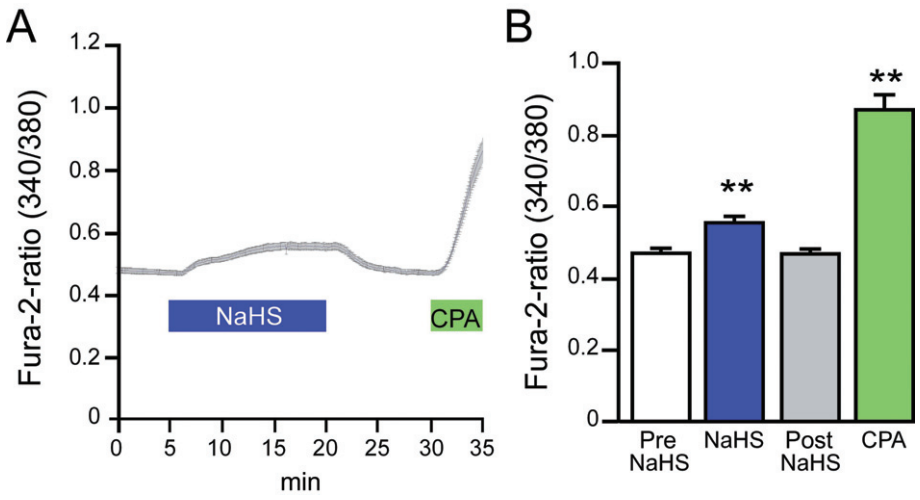


## Figure 6

Effects of NaHS on cytosolic $Ca^{2+}$ concentrations. Changes in cytosolic $Ca^{2+}$ were measured with Fura-2. (A) Fura-2 ratios (340 nm/380 nm) of H441 cells. Depicted are the means ± SEM of $n = 40$ cells. NaHS (1 mM, blue bar) led to a reversible increase in Fura-2 ratios. CPA was used as a positive control. (B) Statistical analysis from data shown in (A). Depicted are Fura-2 ratios before NaHS application (pre NaHS), 15 min after NaHS (NaHS), 10 min after wash-out of NaHS (post NaHS), and 5 min after CPA-administration (CPA). $^{**}P < 0.01$.

inhibiting basolateral $K^+$ channels with lidocaine (3 mM) reduced amiloride-sensitive currents, and thus $Na^+$ transport of intact H441 monolayers from 12.0 ± 1.4 μA·cm$^{-2}$ to 9.5 ± 1 μA·cm$^{-2}$ ($n = 5$, $P < 0.05$).

### *Effects of $H_2S$ on basolateral $K^+$ channels*

Modulation of $K^+$ channel activity can indirectly affect $Na^+$ transport and $Na^+/K^+$-ATPase currents in H441 cells, therefore, we investigated whether or not $H_2S$ has an effect on $K^+$ channels in the basolateral membrane of H441 monolayers (Figure 8C–E). Monolayers were exposed to an apical to basolateral $K^+$ gradient. To exclude any contribution of the main $Na^+$ transporting molecules, amiloride and ouabain were also applied. Monolayers were apically permeabilized with nystatin, which resulted in a current increase from 7.0 ± 1.2 μA·cm$^{-2}$ to 11.1 ± 1.3 μA·cm$^{-2}$ ($n = 10$, $P < 0.005$). This current increase was sensitive to the non-specific $K^+$ channel blocker lidocaine (3 mM, Figure 8C). These conditions reflect the movement of $K^+$ ions via basolaterally located $K^+$ channels. The lidocaine-sensitive fraction of the $I_{SC}$ ($I_{lido}$) under control conditions was 3.4 ± 0.6 μA·cm$^{-2}$. NaHS significantly decreased $I_{lido}$ to 0.4 ± 0.4 μA·cm$^{-2}$ ($n = 5$, $P < 0.01$) (Figure 8D, E).

Additionally, the type of basolateral $K^+$ channels affected by $H_2S$ was investigated and their contribution to the indirect inhibition of transepithelial $Na^+$ transport. Inhibitors of the three classes of $K^+$ channels were employed and their effects on $I_{ami}$ investigated (Figure 9A). The basolateral application of glibenclamide (100 μM), a blocker of ATP-sensitive $K^+$ ($K_{ATP}$) channels, did not change $I_{ami}$ of H441 monolayers. Normalized values of $I_{ami}$ were 1 before and 1.06 ± 0.05 after application of glibenclamide ($n = 5$, $P = 0.25$, Figure 9A). By contrast, basolateral exposure to XE991 (100 μM), a blocker of voltage-gated $K^+$ ($K_V$) channels (Greenwood *et al.*, 2009), significantly decreased normalized $I_{ami}$ from 1 to 0.73 ± 0.04 ($n = 4$, $P < 0.01$; Figure 9A). Lastly, tetrapentylammonium (TPeA), a drug that preferentially inhibits calcium-dependent $K^+$ ($K_{Ca}$) channels dramatically decreased $Na^+$ transport when applied to the basolateral compartment (300 μM). Normalized values of $I_{ami}$ significantly decreased from 1 to 0.43 ± 0.03 ($n = 5$, $P < 0.01$; Figure 9A). These data indicate that ~25% of the $Na^+$ current in H441 monolayers is maintained by active $K_V$ channels and ~65% by active $K_{Ca}$ channels, rather than $K_{ATP}$ channels. Subsequently, the effects of $H_2S$ on $K_V$ and $K_{Ca}$ channels were investigated. In the presence of the $K_V$ inhibitor XE991 (100 μM, basolateral side), NaHS (300 μM, apical) still decreased $I_{ami}$ to the same extent as in control recordings without XE991 (Figure 9B, C). The NaHS-induced currents, which were calculated as relative inhibition of $I_{ami}$ (Figure 9C), were 44.65 ± 3.98% under control conditions and 44.3 ± 1.94% in the presence of XE991 ($n = 4$, $P = 0.94$; Figure 9C). By contrast, TPeA decreased $I_{ami}$ to the same extent as NaHS (Figure 9D, E) and significantly reduced NaHS-induced currents from 51.01 ± 2.32% to 34.38 ± 2.79% ($n = 5$, $P < 0.01$; Figure 9F). These data indicate that $H_2S$ preferentially inhibits $K_{Ca}$ channels, and thus indirectly decreases amiloride-sensitive transepithelial $Na^+$ absorption.

## Discussion and conclusions

The results presented here demonstrate that $H_2S$ decreases transepithelial $Na^+$ absorption across human H441 airway epithelial cells (Figure 1) and native tracheal preparations of pigs and mice (Figure 2). The $IC_{50}$ value for the donor molecule NaHS was determined as 146 μM, which will correspond to an $IC_{50}$ of free $H_2S$ of ~50 μM. The 'real' physiological concentration of $H_2S$ is still debatable, because a variety of $H_2S$ concentrations in tissues have been determined – ranging from <1 μM up to more than 100 μM (for

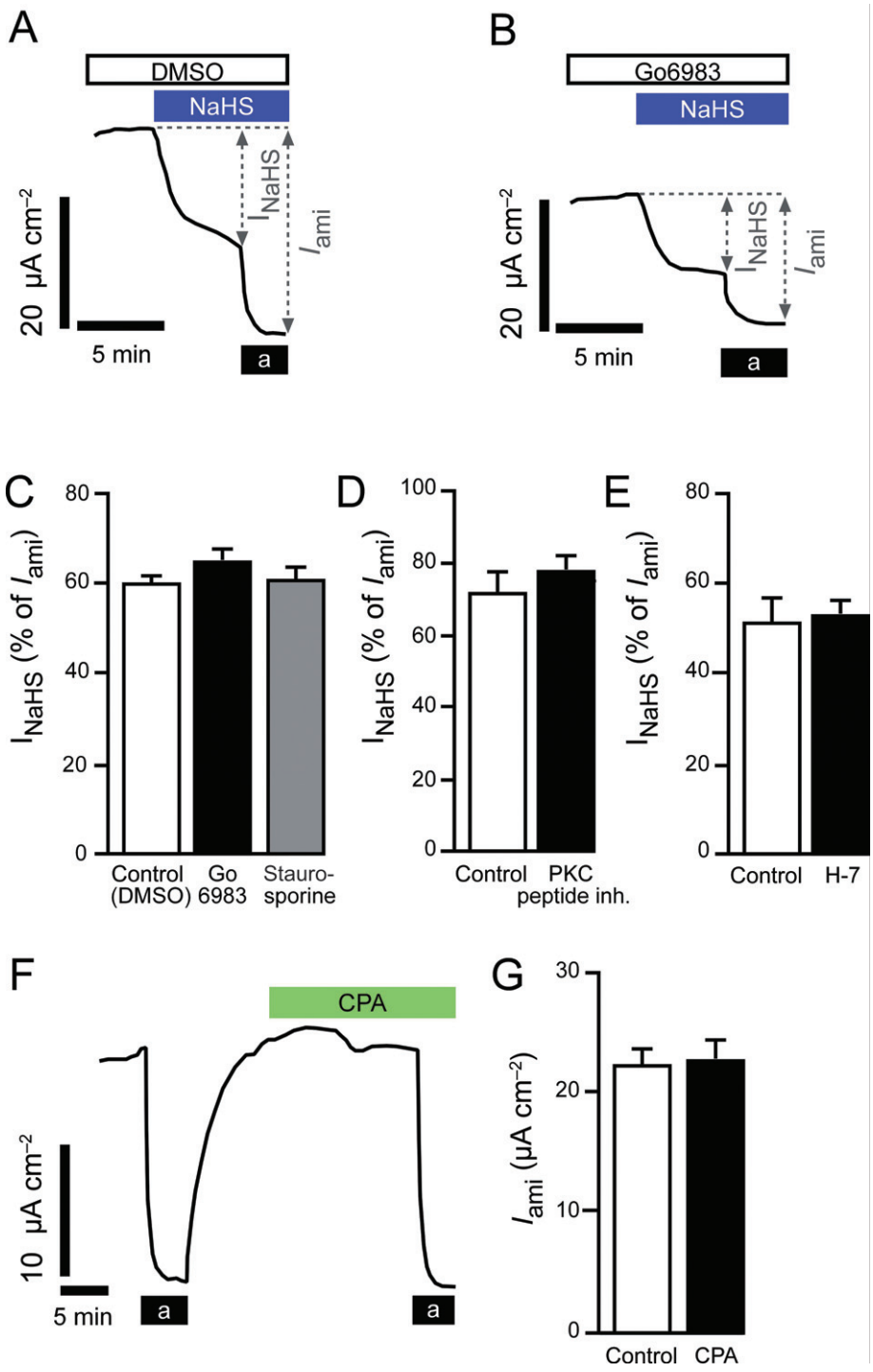


## Figure 7

Effects of NaHS on $Ca^{2+}$/protein kinase C signalling. (A, B) Representative current traces of H441 cells in Ussing chambers. Cells were incubated with solvent (DMSO), or the PKC inhibitor Go6983 (5 µM), 1 h before the start of experiments at 37°C. In Ussing chamber experiments, all drugs were also present in the apical and basolateral perfusion solutions. Note that Go6983 generally decreased short-circuit currents; however, the effect of NaHS (300 µM) was still present. 'a' = amiloride (10 µM). (C–E) Statistical analysis of experiments similar to those shown in (A). Depicted are NaHS-mediated currents ($I_{NaHS}$) relative to total amiloride-sensitive currents ($I_{ami}$). Go6983 (5 µM) and staurosporine (200 nM) did not significantly affect $I_{NaHS}$ ($n = 5$, $P = 0.2955$, one-way ANOVA). Similarly, the PKC peptide inhibitor (60 µM, $n = 4$; $P = 0.42$) or H-7 (20 µM; $n = 5$; $P = 0.79$) did not significantly affect $I_{NaHS}$. (F) The effect of CPA on ion currents of H441 monolayers in Ussing chambers. Firstly, amiloride (a) was applied to estimate baseline $I_{ami}$. After wash-out, CPA (10 µM) was applied to the apical compartment and after 10 min, $I_{ami}$ was determined again. (G) There were not significant changes in $I_{ami}$ induced by CPA ($n = 5$; $P = 0.41$).

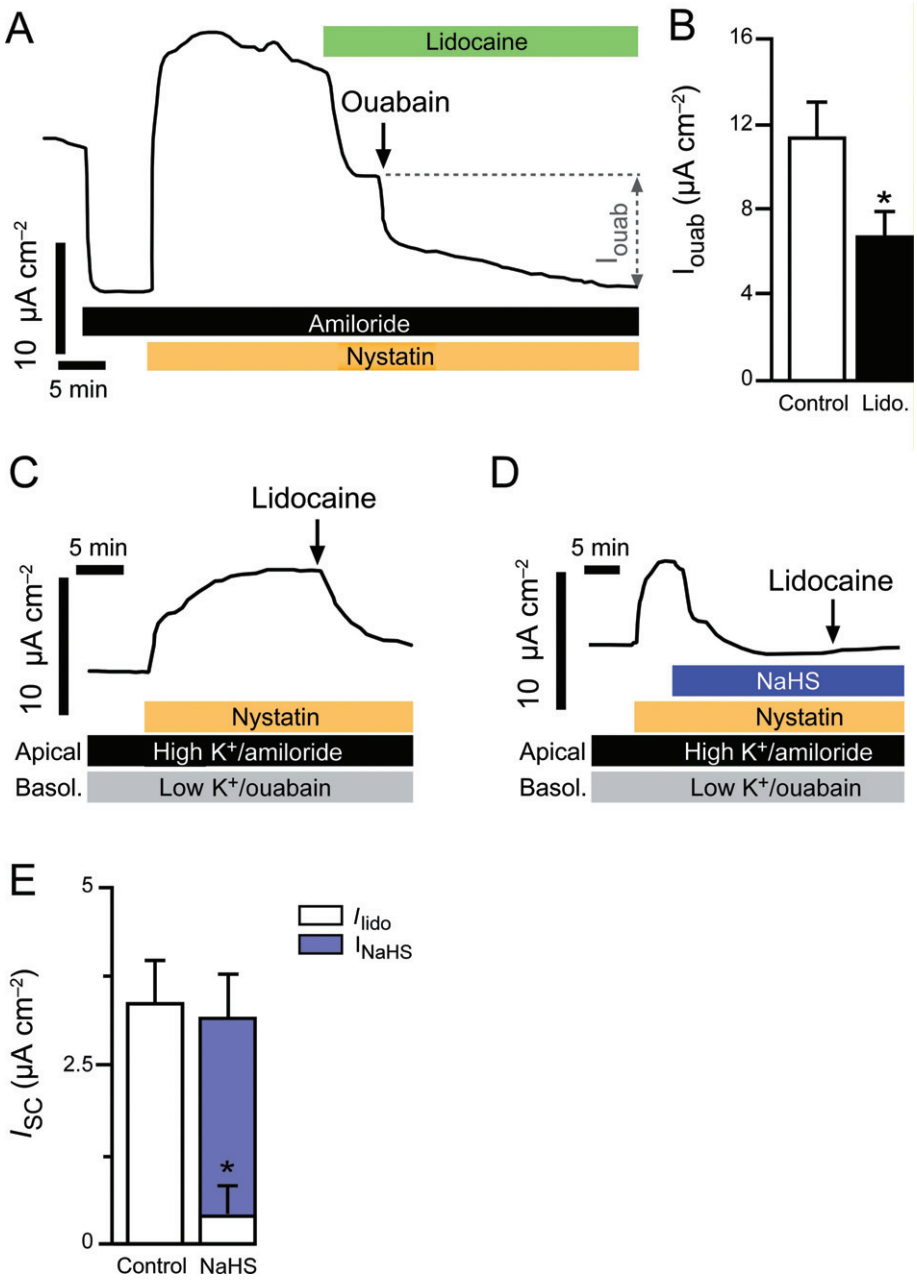


## Figure 8

Regulation of the $Na^+/K^+$-ATPase by $K^+$ channels and effects of NaHS on basolateral $K^+$ channels in H441 cells. (A) Representative current trace of an experiment similar to those explained in Figure 4. Note that the basolateral application of lidocaine (3 mM) reduced ouabain-sensitive currents ($I_{ouab}$) on apically permeabilized H441 monolayers. (B) Statistical evaluation of experiments shown in (A). Basolateral application of lidocaine significantly decreased $I_{ouab}$ compared with control experiments without lidocaine (current trace not shown). *$P < 0.05$. (C) H441 monolayers in Ussing chambers were apically bathed with a high $K^+$ solution containing amiloride (10 µM). The basolateral bath contained low $K^+$ and ouabain (1 mM). Monolayers were perfused for at least 10 min with these solutions (not shown). After plateau conditions had been reached, nystatin (75 µM) was apically applied to permeabilize the apical membrane. The resulting current increase was sensitive to the basolateral application of lidocaine (3 mM). (D) Similar experiment to those shown in (A). After permeabilization with nystatin, NaHS (300 µM) was applied to the apical bath. After plateau conditions had been reached, lidocaine (3 mM) was then applied to the basolateral bath. (E) Statistical analysis from experiments shown in (A and B). Depicted are lidocaine-sensitive currents ($I_{lido}$) and the NaHS-sensitive current ($I_{NaHS}$).

review see Olson, 2011). However, it has to be mentioned that most studies determined $H_2S$ concentrations in plasma or whole-tissue homogenates. Even though the current view is that physiological concentrations of $H_2S$ are in the nanomolar to lower micromolar range (Olson, 2011), local $H_2S$ concentrations might be higher – depending on the place and activity of $H_2S$-generating enzymes. Whether or not endogenously synthesized $H_2S$ is a real physiological regulator of

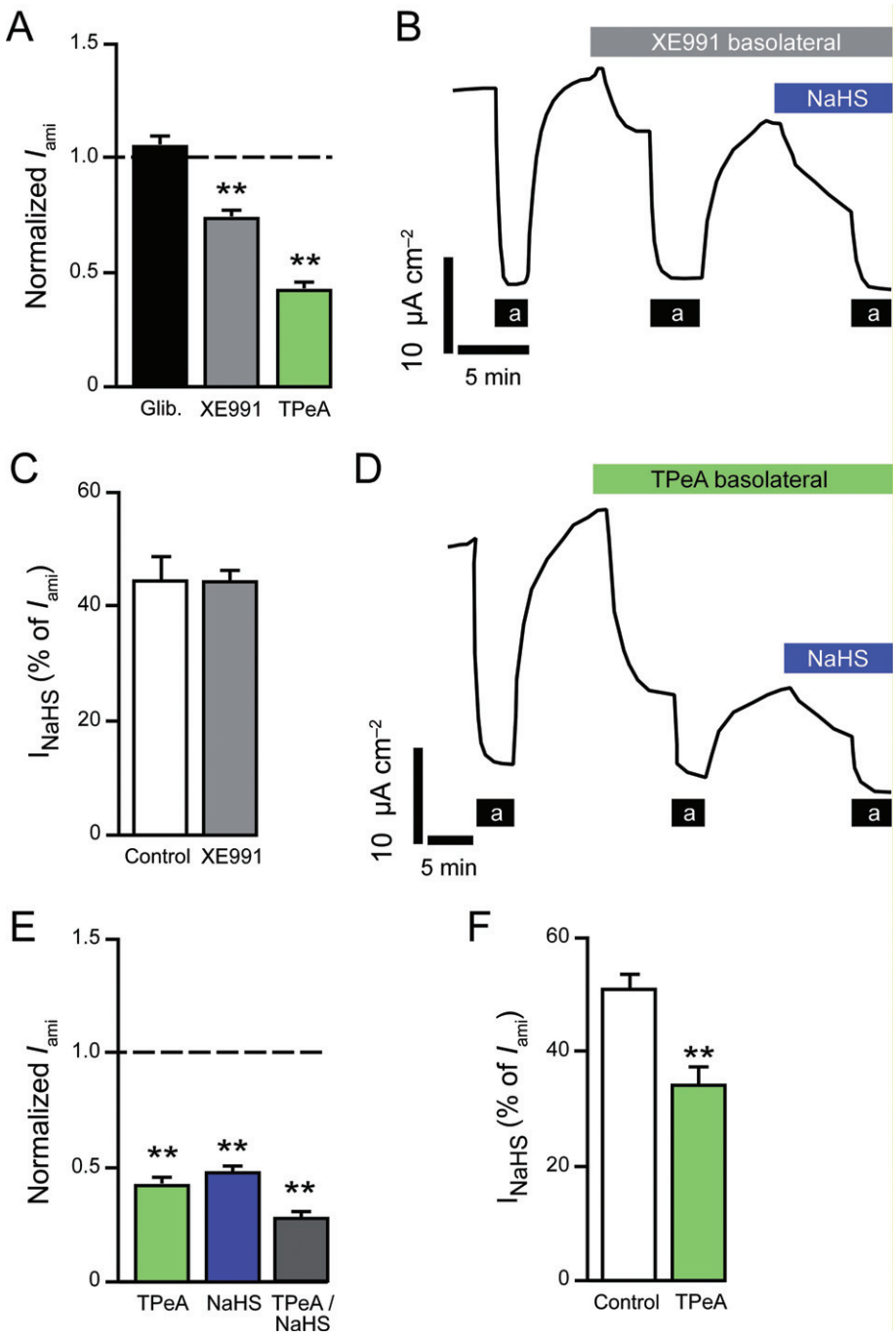


## Figure 9

Contribution of $K_{ATP}$, $K_V$ and $K_{Ca}$ channels to $H_2S$-mediated effects. (A) Effects of basolaterally applied $K^+$ channel inhibitors on amiloride-sensitive currents ($I_{ami}$) of H441 monolayers in Ussing chambers. Depicted are normalized values of $I_{ami}$, which were obtained by normalization of $I_{ami}$ with inhibitors (one inhibitor per monolayer) to baseline $I_{ami}$ without inhibitors (normalized to '1', shown as dashed line). Glibenclamide (100 µM, Glib.) did not affect $I_{ami}$ ($n = 5$, $P = 0.25$). XE991 (100 µM) and TPeA both significantly decreased $I_{ami}$ ($n = 4$, and $n = 5$, respectively; $^{**}P < 0.01$). (B) Original current trace from H441 monolayers in Ussing chambers. The basolateral application of XE991 (100 µM) decreased amiloride-sensitive currents (amiloride = a); however, there was still a prominent effect of NaHS (300 µM, apical application). (C) Statistical analysis from experiments shown in (B) and from control recordings without XE991 (not shown). Depicted are NaHS-mediated currents ($I_{NaHS}$), which were normalized (as explained in Figure 7). XE991 had no significant effect on the $I_{NaHS}$ ($n = 4$, $P = 0.94$). (D) Similar recordings to those shown in (B), with basolateral application of TPeA (300 µM). (E) Statistical analysis of experiments shown in (D). Depicted are normalized values of $I_{ami}$, which were obtained by normalization of $I_{ami}$ with TPeA, NaHS or a combination of both to baseline $I_{ami}$ without drugs (normalized to '1', shown as dashed line). Statistics represent the comparison between normalized $I_{ami}$ during drug exposure with respect to baseline normalized $I_{ami}$. Note that TPeA decreased $I_{ami}$ to a similar extent as NaHS when applied without TPeA (original traces not shown); $^{**}P < 0.01$. (F) TPeA significantly decreased the NaHS-mediated currents ($I_{NaHS}$, $n = 5$, $^{**}P < 0.01$).

transepithelial $Na^+$ transport is an important question that needs to be addressed. We were able to detect mRNA transcripts for the $H_2S$-generating enzymes CBS and CSE in H441 cells (data not shown). However, administration of the CSE inhibitor β-cyanoalanine (500 μM apical), the CBS inhibitor amino-oxyacetate (1 mM, apical) or a combination of both, in concentrations that were demonstrated to inhibit CBS/CSE (Mok *et al.*, 2004; Hughes *et al.*, 2009), did not significantly increase amiloride-sensitive $Na^+$ absorption by H441 cells within 30 min (data not shown). This does not speak in favour of a tonic, inhibitory effect of $H_2S$ that is produced directly in the epithelium. Nevertheless, $H_2S$ production might be low under basal conditions or $H_2S$ might originate from other lung compartments, such as the endothelium or even the plasma, and might thereby affect epithelial $Na^+$ transport. This important question warrants further investigations.

Amiloride-sensitive $Na^+$ channels, such as ENaC, were not directly affected by $H_2S$ (Figure 3), whereas $Na^+/K^+$-ATPase currents were decreased (Figure 4). This observation is in line with a recent study that described decreased $Na^+/K^+$-ATPase currents due to NaHS in distal colonic epithelia (Pouokam and Diener, 2011). The $Na^+/K^+$-ATPase creates the $Na^+$ gradient that drives the entry of $Na^+$ ions through $Na^+$ channels located at the apical membrane of epithelial cells. Thus, although in the present study, $H_2S$ did not directly inhibit $Na^+$ channels, the inhibition of the $Na^+/K^+$-ATPase by $H_2S$ will indirectly decrease apical $Na^+$ uptake through those ion channels and decrease amiloride-sensitive transepithelial $Na^+$ transport (Figures 1 and 2).

The decreased $Na^+/K^+$-ATPase currents in H441 cells were not the result of endocytosis of $Na^+/K^+$-ATPase molecules from the plasma membrane, because the abundance of the $Na^+/K^+$-ATPase in the membrane was unchanged (Figure 5).

The $H_2S$-induced inhibition of $Na^+$ transport by H441 cells was not accompanied by a decrease in cellular ATP, which might have represented a mechanism for an indirect $Na^+/K^+$-ATPase inhibition and thus a decreased $Na^+$ transport. This finding is of particular importance because $H_2S$ concentrations employed in the present study (~100 μM of free $H_2S$) are regarded to be in a range that might inhibit mitochondrial cytochrome c oxidase (Olson, 2011). However, the present results indicate that $H_2S$ can impair $Na^+/K^+$-ATPase activity independently of metabolic depletion and is thus a physiological, rather than a toxicological observation. This finding is in accordance with previous studies, which demonstrated that only a drastic depletion of ATP would alter $Na^+/K^+$-ATPase activity (Boldyrev *et al.*, 1991; Woollhead *et al.*, 2005). Nevertheless, it remains possible that $H_2S$ changes the ATP : AMP ratio, which will activate AMP-activated protein kinase (AMPK) and eventually inhibit the $Na^+/K^+$-ATPase (Woollhead *et al.*, 2005). However, in H441 cells, AMPK inhibits the $Na^+/K^+$-ATPase due to activation of PKC and endocytosis (data not shown). As both signalling pathways did not contribute to the $H_2S$ effect (Figures 5 and 7), a contribution of AMPK to the $H_2S$ induced $Na^+/K^+$-ATPase inhibition is unlikely.

As the abundance of $Na^+/K^+$-ATPase in the membrane was unaffected by $H_2S$, the decreased ouabain-sensitive current across the basolateral membrane is likely to be the result of decreased $Na^+/K^+$-ATPase activity. Therefore, signalling pathways that lead to alterations in $Na^+/K^+$-ATPase activity were investigated. $H_2S$ elicited a small and reversible increase in cytosolic $Ca^{2+}$ concentrations (Figure 6). This is in line with observations on rat colonic epithelia (Hennig and Diener, 2009). However, this increase in $Ca^{2+}$ concentration did not account for the observed inhibition of $Na^+$ transport, because CPA had no effect on $I_{ami}$ (Figure 7). Furthermore, the $H_2S$-mediated current inhibition was not affected by inhibitors of PKC or broad-spectrum kinase inhibitors (Figure 7). A putative direct interaction of $H_2S$ with the $Na^+/K^+$-ATPase, as indicated by measurement of ATP hydrolysis *in vitro*, was also not observed.

The present results show that $H_2S$ blocked $K^+$ channels located at the basolateral membrane of the epithelial cells (Figure 8). Due to their effect on electrochemical gradients, $K^+$ channels are important regulators of transepithelial $Na^+$ fluxes (Greenwood *et al.*, 2009). A block of basolateral $K^+$ conductance will eventually depolarize the apical membrane potential. This will result in a decreased electrical driving-force for $Na^+$ entry through apical ion channels. Furthermore, there is a coupling between the $Na^+/K^+$-ATPase and $K^+$ channels, which recycle the $K^+$ ions that enter the cells due to $Na^+/K^+$-ATPase activity. It has been demonstrated that the activity of the $Na^+/K^+$-ATPase is coupled to $K^+$ flux at the basolateral membrane (Beck *et al.*, 1994; Mauerer *et al.*, 1998). This coupling might prevent loss of $K^+$, when $Na^+/K^+$-ATPase activity is low. *Vice versa*, it is hypothesized that inhibition of $K^+$ channels also decreases $Na^+/K^+$-ATPase activity to prevent a $K^+$ loading of cells. This possibility is supported by the finding that the block of basolateral $K^+$ channels (with lidocaine, Inglis *et al.*, 2007) rapidly inhibits ouabain-sensitive currents of apically permeabilized H441 monolayers (Figure 8). Both events, depolarizing the apical membrane as well as indirectly impairing $Na^+/K^+$-ATPase activity, will result in inhibition of transepithelial $Na^+$ transport.

In accordance with this assumption, a block of basolateral $K^+$ channels decreased $Na^+$ absorption across intact H441 monolayers (Figure 9). $K_{ATP}$ channels were not active in the basolateral membrane of H441 monolayers, because the inhibitor glibenclamide was ineffective. Thus, $K_{ATP}$ channels, which were shown to be sensitive to $H_2S$ (Tang *et al.*, 2010), cannot account for the $H_2S$-mediated effects. Experiments with XE991 and TPeA (inhibitors of $K_V$ and $K_{Ca}$ channels, respectively) revealed that $Na^+$ transport across H441 cells is maintained by active $K_V$ and $K_{Ca}$ channels. The effect of $H_2S$ was not sensitive to XE991, however, the inhibition of $K_{Ca}$ channels mimicked and decreased the effect of $H_2S$ on $Na^+$ transport (Figure 9). This finding is in accordance to studies by Kemp and colleagues, who demonstrated inhibition of human $BK_{Ca}$ channels by $H_2S$ (Telezhkin *et al.*, 2009). Although the precise mechanism of $H_2S$'s action on these channels is unknown, the effects of $H_2S$ on $BK_{Ca}$ channels were observed in cell-free membrane patches (Telezhkin *et al.*, 2010), and are probably independent of soluble signalling mediators. There is recent evidence that $H_2S$ is able to convert SH-groups of proteins to SSH-groups, a mechanism that has been termed S-sulfhydration (Mustafa *et al.*, 2009). S-sulfhydration has been described for intermediate and short conductance $K_{Ca}$ channels (Mustafa *et al.*, 2009). Hence, we speculate that the observed inhibition of $K_{Ca}$ channels, due to $H_2S$, is the result of S-sulfhydration.

Taken together, the data presented in this study indicate that $H_2S$ blocks $K_{Ca}$ channels located in the basolateral membrane and indirectly impairs transepithelial $Na^+$ absorption by possibly altering the apical membrane potential, as well as $Na^+/K^+$-ATPase activity.

The finding that $H_2S$ decreased pulmonary $Na^+$ absorption has important pharmacological implications. In the distal lung, decreased $Na^+$ absorption across the alveolar epithelium leads to decreased alveolar fluid clearance and the promotion of oedema formation. Interestingly, a characteristic of patients with $H_2S$ poisoning is the development of pulmonary oedema, which was also observed in patients after prolonged exposure to low concentrations of $H_2S$ (Cordasco and Stone, 1973). The results presented herein have provided a novel molecular mechanism for this observation.

Furthermore, $H_2S$ is, due to its anti-inflammatory properties, suggested as a potential therapeutic option for the treatment of inflammatory lung diseases, including ALI (Esechie *et al.*, 2009; Otulakowski and Kavanagh, 2010). Although $H_2S$ gas is unlikely to become a therapeutic tool, there are various $H_2S$-donating molecules (Olson, 2011) that would allow the pharmacological administration of $H_2S$. However, aside from inflammation, the development of pulmonary oedema is a hallmark of patients with ALI, or the more severe acute respiratory distress syndrome (ARDS; Ware and Matthay, 2000). Oedema occurrence in ALI/ARDS patients is *inter alia* associated with an impaired alveolar fluid clearance (Ware and Matthay, 2001). Impairment of transepithelial $Na^+$ transport by $H_2S$ is an important observation that needs to be taken into consideration when considering $H_2S$ as a therapeutic option in ALI/ARDS (Otulakowski and Kavanagh, 2010), even when evaluating $H_2S$ concentrations that do not lead to metabolic depletion.

Apart from the potential deleterious effects of $H_2S$ with respect to oedema formation, $H_2S$ might, by contrast, represent an interesting pharmacological target in situations where a hyperactive $Na^+$ transport is present. In airway epithelia, increased $Na^+$ absorption can promote cystic fibrosis-like lung disease (Mall *et al.*, 2004). In the kidneys, a hereditary form of hypertension (Liddle syndrome) is reasoned by an ENaC mutation that leads to $Na^+$ hyperabsorption from the primary urine and consequently increases blood volume and pressure (Firsov *et al.*, 1996; Kellenberger and Schild, 2002). In both cases, blocking $Na^+$ transport by increasing endogenous $H_2S$ production might provide a new pharmacological approach.

In conclusion, the data presented here suggest that the gasotransmitter $H_2S$ interferes with basolateral $K^+$ channels in lung epithelial cells, and thereby indirectly impairs transepithelial $Na^+$ transport. $H_2S$ might therefore be a novel regulator of pulmonary $Na^+$ absorption, and its signalling mechanisms might represent novel pharmacological targets for the investigation of drugs that regulate pulmonary $Na^+$ and water homeostasis.

## Acknowledgements

The authors thank Alexandra Erb, Carolin Brössel, Philip Glombik and Denis Revskij for the help with some experiments; Sarah Kessler for expert advice concerning whole-cell patch-clamp experiments; and Monika I. Hollenhorst and Katrin Richter for the help with tracheal preparations. Mirjam Buss and Anja Schnecko are acknowledged for excellent technical assistance. We are grateful to the group of Prof. Martin Diener (Institute of Veterinary Physiology at the University of Giessen) for enabling us to perform calcium imaging experiments and their outstanding support. This work was supported by the *Deutsche Forschungsgemeinschaft*, AL-1453/1-1 (to MA and WGC). KDU was supported by the RISE program of the German Academic Exchange Service (DAAD).

## Conflict of interest

The authors declare no conflict of interest.

## References

Albert AP, Woollhead AM, Mace OJ, Baines DL (2008). AICAR decreases the activity of two distinct amiloride-sensitive $Na^+$-permeable channels in H441 human lung epithelial cell monolayers. Am J Physiol Lung Cell Mol Physiol 295: L837–L848.

Alexander SPH, Mathie A, Peters JA (2011). Guide to receptors and channels (GRAC), 5th edn. Br J Pharmacol 164 (Suppl. 1): S1–S324.

Althaus M, Fronius M, Buchäckert Y, Vadász I, Clauss WG, Seeger W *et al.* (2009). Carbon monoxide rapidly impairs alveolar fluid clearance by inhibiting epithelial sodium channels. Am J Respir Cell Mol Biol 41: 639–650.

Althaus M, Pichl A, Clauss WG, Seeger W, Fronius M, Morty RE (2010). Nitric oxide inhibits highly selective sodium channels and the $Na^+/K^+$-ATPase in H441 cells. Am J Respir Cell Mol Biol 44: 53–65.

Althaus M, Clauss WG, Fronius M (2011). Amiloride-sensitive sodium channels and pulmonary edema. Pulm Med 2011: 830320.

Aslami H, Heinen A, Roelofs JJTH, Zuurbier CJ, Schultz MJ, Juffermans NP (2010). Suspended animation inducer hydrogen sulfide is protective in an in vivo model of ventilator-induced lung injury. Intensive Care Med 36: 1946–1952.

Barrett-Jolley R, Davies NW (1997). Kinetic analysis of the inhibitory effect of glibenclamide on KATP channels of mammalian skeletal muscle. J Membr Biol 155: 257–262.

Beck JS, Laprade R, Lapointe JY (1994). Coupling between transepithelial Na transport and basolateral K conductance in renal proximal tubule. Am J Physiol 266: F517–F527.

Becq F, Mall MA, Sheppard DN, Conese M, Zegarra-Moran O (2011). Pharmacological therapy for cystic fibrosis: from bench to bedside. J Cyst Fibros 10 (Suppl. 2): S129–S145.

Bertorello AM, Aperia A, Walaas SI, Nairn AC, Greengard P (1991). Phosphorylation of the catalytic subunit of Na+,K(+)-ATPase inhibits the activity of the enzyme. Proc Natl Acad Sci U S A 88: 11359–11362.

Boldyrev AA, Fedosova NU, Lopina OD (1991). The mechanism of the modifying effect of ATP on Na(+)-K+ ATPase. Biomed Sci 2: 450–454.

Brown SG, Gallacher M, Olver RE, Wilson SM (2008). The regulation of selective and nonselective $Na^+$ conductances in H441 human airway epithelial cells. Am J Physiol Lung Cell Mol Physiol 294: L942–L954.

Canessa CM, Schild L, Buell G, Thorens B, Gautschi I, Horisberger JD *et al.* (1994). Amiloride-sensitive epithelial $Na^+$ channel is made of three homologous subunits. Nature 367: 463–467.

Clunes MT, Butt AG, Wilson SM (2004). A glucocorticoid-induced $Na^+$ conductance in human airway epithelial cells identified by perforated patch recording. J Physiol 557: 809–819.

Collman JP, Ghosh S, Dey A, Decréau RA (2009). Using a functional enzyme model to understand the chemistry behind hydrogen sulfide induced hibernation. Proc Natl Acad Sci U S A 106: 22090–22095.

Cordasco EM, Stone FD (1973). Pulmonary edema of environmental origin. Chest 64: 182–185.

Eichholtz T, de Bont DB, de Widt J, Liskamp RM, Ploegh HL (1993). A myristoylated pseudosubstrate peptide, a novel protein kinase C inhibitor. J Biol Chem 268: 1982–1986.

Esechie A, Enkhbaatar P, Traber DL, Jonkam C, Lange M, Hamahata A *et al.* (2009). Beneficial effect of a hydrogen sulphide donor (sodium sulphide) in an ovine model of burn- and smoke-induced acute lung injury. Br J Pharmacol 158: 1442–1453.

Faller S, Ryter SW, Choi AMK, Loop T, Schmidt R, Hoetzel A (2010). Inhaled hydrogen sulfide protects against ventilator-induced lung injury. Anesthesiology 113: 104–115.

Firsov D, Schild L, Gautschi I, Mérillat AM, Schneeberger E, Rossier BC (1996). Cell surface expression of the epithelial Na channel and a mutant causing Liddle syndrome: a quantitative approach. Proc Natl Acad Sci U S A 93: 15370–15375.

Fronius M, Bogdan R, Althaus M, Morty RE, Clauss WG (2010). Epithelial $Na^+$ channels derived from human lung are activated by shear force. Respir Physiol Neurobiol 170: 113–119.

Greenwood IA, Yeung SYM, Hettiarachi S, Andersson M, Baines DL (2009). KCNQ-encoded channels regulate $Na^+$ transport across H441 lung epithelial cells. Pflugers Arch 457: 785–794.

Gschwendt M, Dieterich S, Rennecke J, Kittstein W, Mueller HJ, Johannes FJ (1996). Inhibition of protein kinase C mu by various inhibitors. Differentiation from protein kinase c isoenzymes. FEBS Lett 392: 77–80.

Guo Y, DuVall MD, Crow JP, Matalon S (1998). Nitric oxide inhibits $Na^+$ absorption across cultured alveolar type II monolayers. Am J Physiol 274: L369–L377.

Helms MN, Jain L, Self JL, Eaton DC (2008). Redox regulation of epithelial sodium channels examined in alveolar type 1 and 2 cells patch-clamped in lung slice tissue. J Biol Chem 283: 22875–22883.

Hennig B, Diener M (2009). Actions of hydrogen sulphide on ion transport across rat distal colon. Br J Pharmacol 158: 1263–1275.

Hidaka H, Inagaki M, Kawamoto S, Sasaki Y (1984). Isoquinolinesulfonamides, novel and potent inhibitors of cyclic nucleotide dependent protein kinase and protein kinase C. Biochemistry 23: 5036–5041.

Hollenhorst MI, Lips KS, Weitz A, Krasteva G, Kummer W, Fronius M (2012). Evidence for functional atypical nicotinic receptors that activate $K^+$ dependent $Cl^-$ secretion in mouse tracheal epithelium. Am J Respir Cell Mol Biol 46: 106–114.

Hughes MN, Centelles MN, Moore KP (2009). Making and working with hydrogen sulfide: the chemistry and generation of hydrogen sulfide in vitro and its measurement in vivo: a review. Free Radic Biol Med 47: 1346–1353.

Inglis SK, Brown SG, Constable MJ, McTavish N, Olver RE, Wilson SM (2007). A $Ba^{2+}$-resistant, acid-sensitive $K^+$ conductance in $Na^+$-absorbing H441 human airway epithelial cells. Am J Physiol Lung Cell Mol Physiol 292: L1304–L1312.

Jasti J, Furukawa H, Gonzales EB, Gouaux E (2007). Structure of acid-sensing ion channel 1 at 1.9 A resolution and low pH. Nature 449: 316–323.

Kellenberger S, Schild L (2002). Epithelial sodium channel/degenerin family of ion channels: a variety of functions for a shared structure. Physiol Rev 82: 735–767.

Kerem E, Bistritzer T, Hanukoglu A, Hofmann T, Zhou Z, Bennett W *et al.* (1999). Pulmonary epithelial sodium-channel dysfunction and excess airway liquid in pseudohypoaldosteronism. N Engl J Med 341: 156–162.

Kubo S, Doe I, Kurokawa Y, Kawabata A (2007). Hydrogen sulfide causes relaxation in mouse bronchial smooth muscle. J Pharmacol Sci 104: 392–396.

Lazrak A, Matalon S (2003). cAMP-induced changes of apical membrane potentials of confluent H441 monolayers. Am J Physiol Lung Cell Mol Physiol 285: L443–L450.

Lee SW, Hu YS, Hu LF, Lu Q, Dawe GS, Moore PK *et al.* (2006). Hydrogen sulphide regulates calcium homeostasis in microglial cells. Glia 54: 116–124.

Mace OJ, Woollhead AM, Baines DL (2008). AICAR activates AMPK and alters PIP2 association with the epithelial sodium channel ENaC to inhibit $Na^+$ transport in H441 lung epithelial cells. J Physiol (Lond) 586: 4541–4557.

Macia E, Ehrlich M, Massol R, Boucrot E, Brunner C, Kirchhausen T (2006). Dynasore, a cell-permeable inhibitor of dynamin. Dev Cell 10: 839–850.

Maguire D, MacNamara B, Cuffe JE, Winter D, Doolan CM, Urbach V *et al.* (1999). Rapid responses to aldosterone in human distal colon. Steroids 64: 51–63.

Mall M, Grubb BR, Harkema JR, O'Neal WK, Boucher RC (2004). Increased airway epithelial Na+ absorption produces cystic fibrosis-like lung disease in mice. Nat Med 10: 487–493.

Matalon S, Lazrak A, Jain L, Eaton DC (2002). Invited review: biophysical properties of sodium channels in lung alveolar epithelial cells. J Appl Physiol 93: 1852–1859.

Mathai JC, Missner A, Kügler P, Saparov SM, Zeidel ML, Lee JK *et al.* (2009). No facilitator required for membrane transport of hydrogen sulfide. Proc Natl Acad Sci U S A 106: 16633–16638.

Mauerer UR, Boulpaep EL, Segal AS (1998). Regulation of an inwardly rectifying ATP-sensitive $K^+$ channel in the basolateral membrane of renal proximal tubule. J Gen Physiol 111: 161–180.

McGrath J, Drummond G, McLachlan E, Kilkenny C, Wainwright C (2010). Guidelines for reporting experiments involving animals: the ARRIVE guidelines. Br J Pharmacol 160: 1573–1576.

Mok YY, Atan MS, Yoke Ping C, Zhong Jing W, Bhatia M, Moochhala S *et al.* (2004). Role of hydrogen sulphide in haemorrhagic shock in the rat: protective effect of inhibitors of hydrogen sulphide biosynthesis. Br J Pharmacol 143: 881–889.

Mustafa AK, Gadalla MM, Sen N, Kim S, Mu W, Gazi SK *et al.* (2009). $H_2S$ signals through protein S-sulfhydration. Sci Signal 2: ra72.

Nie HG, Chen L, Han DY, Li J, Song WF, Wei SP *et al.* (2009). Regulation of epithelial sodium channels by cGMP/PKGII. J Physiol (Lond) 587: 2663–2676.

Olson KR (2011). The therapeutic potential of hydrogen sulfide: separating hype from hope. Am J Physiol Regul Integr Comp Physiol 301: R297–R312.

Olson KR, Whitfield NL, Bearden SE, St Leger J, Nilson E, Gao Y *et al*. (2010). Hypoxic pulmonary vasodilation: a paradigm shift with a hydrogen sulfide mechanism. Am J Physiol Regul Integr Comp Physiol 298: R51–R60.

Otulakowski G, Kavanagh BP (2010). Hydrogen sulfide in lung injury: therapeutic hope from a toxic gas? Anesthesiology 113: 4–6.

Pouokam E, Diener M (2011). Mechanisms of actions of hydrogen sulphide on rat distal colonic epithelium. Br J Pharmacol 162: 392–404.

Ramminger SJ, Richard K, Inglis SK, Land SC, Olver RE, Wilson SM (2004). A regulated apical Na(+) conductance in dexamethasone-treated H441 airway epithelial cells. Am J Physiol Lung Cell Mol Physiol 287: L411–L419.

Reiffenstein RJ, Hulbert WC, Roth SH (1992). Toxicology of hydrogen sulfide. Annu Rev Pharmacol Toxicol 32: 109–134.

Rüegg UT, Burgess GM (1989). Staurosporine, K-252 and UCN-01: potent but nonspecific inhibitors of protein kinases. Trends Pharmacol Sci 10: 218–220.

Russell JM, Eaton DC, Brodwick MS (1977). Effects of nystatin on membrane conductance and internal ion activities in Aplysia neurons. J Membr Biol 37: 137–156.

Ryter SW, Morse D, Choi AMK (2007). Carbon monoxide and bilirubin: potential therapies for pulmonary/vascular injury and disease. Am J Respir Cell Mol Biol 36: 175–182.

Stipanuk MH, Beck PW (1982). Characterization of the enzymic capacity for cysteine desulphhydration in liver and kidney of the rat. Biochem J 206: 267–277.

Tamaoki T, Nomoto H, Takahashi I, Kato Y, Morimoto M, Tomita F (1986). Staurosporine, a potent inhibitor of phospholipid/Ca++dependent protein kinase. Biochem Biophys Res Commun 135: 397–402.

Tan CD, Selvanathar IA, Baines DL (2011). Cleavage of endogenous γENaC and elevated abundance of αENaC are associated with increased Na(+) transport in response to apical fluid volume expansion in human H441 airway epithelial cells. Pflugers Arch 462: 431–441.

Tang G, Wu L, Wang R (2010). Interaction of hydrogen sulfide with ion channels. Clin Exp Pharmacol Physiol 37: 753–763.

Taussky HH, Shorr E (1953). A microcolorimetric method for the determination of inorganic phosphorus. J Biol Chem 202: 675–685.

Telezhkin V, Brazier SP, Cayzac S, Müller CT, Riccardi D, Kemp PJ (2009). Hydrogen sulfide inhibits human BK(Ca) channels. Adv Exp Med Biol 648: 65–72.

Telezhkin V, Brazier SP, Cayzac SH, Wilkinson WJ, Riccardi D, Kemp PJ (2010). Mechanism of inhibition by hydrogen sulfide of native and recombinant BKCa channels. Respir Physiol Neurobiol 172: 169–178.

Wang HS, Pan Z, Shi W, Brown BS, Wymore RS, Cohen IS *et al*. (1998). KCNQ2 and KCNQ3 potassium channel subunits: molecular correlates of the M-channel. Science 282: 1890–1893.

Wang HS, Brown BS, McKinnon D, Cohen IS (2000). Molecular basis for differential sensitivity of KCNQ and I(Ks) channels to the cognitive enhancer XE991. Mol Pharmacol 57: 1218–1223.

Wang R (2002). Two's company, three's a crowd: can $H_2S$ be the third endogenous gaseous transmitter? FASEB J 16: 1792–1798.

Ware LB, Matthay MA (2000). The acute respiratory distress syndrome. N Engl J Med 342: 1334–1349.

Ware LB, Matthay MA (2001). Alveolar fluid clearance is impaired in the majority of patients with acute lung injury and the acute respiratory distress syndrome. Am J Respir Crit Care Med 163: 1376–1383.

Wesch D, Miranda P, Afonso-Oramas D, Althaus M, Castro-Hernández J, Dominguez J *et al*. (2010). The neuronal-specific SGK1.1 kinase regulates {delta}-epithelial $Na^+$ channel independently of PY motifs and couples it to phospholipase C signaling. Am J Physiol Cell Physiol 299: C779–C790.

Wilkinson WJ, Benjamin AR, de Proost I, Orogo-Wenn MC, Yamazaki Y, Staub O *et al*. (2011). Alveolar epithelial CNGA1 channels mediate cGMP-stimulated, amiloride-insensitive, lung liquid absorption. Pflugers Arch 462: 267–279.

Woollhead AM, Scott JW, Hardie DG, Baines DL (2005). Phenformin and 5-aminoimidazole-4-carboxamide-1-beta-D-ribofuranoside (AICAR) activation of AMP-activated protein kinase inhibits transepithelial $Na^+$ transport across H441 lung cells. J Physiol 566: 781–792.

Woollhead AM, Sivagnanasundaram J, Kalsi KK, Pucovsky V, Pellatt LJ, Scott JW *et al*. (2007). Pharmacological activators of AMP-activated protein kinase have different effects on $Na^+$ transport processes across human lung epithelial cells. Br J Pharmacol 151: 1204–1215.